

Graph Estimation From Multi-attribute Data

Mladen Kolar*, Han Liu[†] and Eric P. Xing[‡]

Abstract

Many real world network problems often concern multivariate nodal attributes such as image, textual, and multi-view feature vectors on nodes, rather than simple univariate nodal attributes. The existing graph estimation methods built on Gaussian graphical models and covariance selection algorithms can not handle such data, neither can the theories developed around such methods be directly applied. In this paper, we propose a new principled framework for estimating graphs from multi-attribute data. Instead of estimating the partial correlation as in current literature, our method estimates the partial canonical correlations that naturally accommodate complex nodal features. Computationally, we provide an efficient algorithm which utilizes the multi-attribute structure. Theoretically, we provide sufficient conditions which guarantee consistent graph recovery. Extensive simulation studies demonstrate performance of our method under various conditions. Furthermore, we provide illustrative applications to uncovering gene regulatory networks from gene and protein profiles, and uncovering brain connectivity graph from functional magnetic resonance imaging data.

Keywords: Graphical model selection; Multi-attribute data; Network analysis; Partial canonical correlation.

1 Introduction

In many modern problems, we are interested in studying a network of entities with multiple attributes rather than a simple univariate attribute. For example, when an entity represents a person in a social network, it is widely accepted that the nodal attribute is most naturally a vector with many personal information including demographics, interests, and other features, rather than merely a single attribute, such as a binary vote as assumed in the current literature of social graph estimation based on Markov random fields (Banerjee et al., 2008, Kolar et al., 2010). In another example, when an entity represents a gene in a gene regulation network, modern data acquisition technologies

*Machine Learning Department, Carnegie Mellon University, Pittsburgh, PA 15217, USA; e-mail: mladenk@cs.cmu.edu.

[†]Department of Operations Research and Financial Engineering, Princeton University, Princeton, NJ 08544, USA; e-mail: hanliu@princeton.edu

[‡]Machine Learning Department, Carnegie Mellon University, Pittsburgh, PA 15217, USA; e-mail: epxing@cs.cmu.edu.

allow researchers to measure the activities of a single gene in a high-dimensional space, such as an image of the spatial distribution of the gene expression, or a multi-view snapshot of the gene activity such as mRNA and protein abundances, rather than merely a single attribute such as an expression level, which is assumed in the current literature on gene graph estimation based on Gaussian graphical models (Peng et al., 2009). Indeed, it is somewhat surprising that existing research on graph estimation remains largely blinded to the analysis of multi-attribute data that are prevalent and widely studied in the network community. Existing algorithms and theoretical analysis relies heavily on covariance selection using graphical lasso, or penalized pseudo-likelihood. They can not be easily extended to graphs with multi-variate nodal attributes.

In this paper, we present a study on graph estimation from multi-attribute data, in an attempt to fill the gap between the practical needs and existing methodologies from the literature. Under a Gaussian graphical model, one assumes that a p -dimensional random vector $X \in \mathbb{R}^p$ follows a multivariate Gaussian distribution with the mean μ and covariance matrix Σ , with each component of the vector corresponding to a node in the graph. Based on n independent and identically distributed observations, one can estimate an undirected graph $G = (V, E)$, where the node set V corresponds to the p variables, and the edge set E describes the conditional independence relationships among the variables, that is, variables X_a and X_b are conditionally independent given all the remaining variables if $(a, b) \notin E$. Given multi-attribute data, this approach is clearly invalid, because it naively translates to estimating one graph per attribute. A subsequent integration of all such graphs to a summary graph on the entire dataset may lead to unclear statistical interpretation.

We consider the following new setting for estimating a multi-attribute graph. In this setting, we consider a “stacked” long random vector $X = (X_1^T, \dots, X_p^T)^T$ where $X_1 \in \mathbb{R}^{k_1}, \dots, X_p \in \mathbb{R}^{k_p}$ are themselves random vectors that jointly follow a multivariate Gaussian distribution with mean $\mu = (\mu_1, \dots, \mu_p)^T$ and covariance matrix Σ^* , which is partitioned as

$$\Sigma^* = \begin{pmatrix} \Sigma_{11}^* & \cdots & \Sigma_{1p}^* \\ \vdots & \ddots & \vdots \\ \Sigma_{p1}^* & \cdots & \Sigma_{pp}^* \end{pmatrix}, \quad (1)$$

with $\Sigma_{ij}^* = \text{Cov}(X_i, X_j)$. Without loss of generality, we assume $\mu = 0$. Let $G = (V, E)$ be a graph with the vertex set $V = \{1, \dots, p\}$ and the set of edges $E \subseteq V \times V$ that encodes the conditional independence relationships among $(X_a)_{a \in V}$. That is, each node $a \in V$ of the graph G corresponds to the random vector X_a and there is no edge between nodes a and b in the graph if and only if X_a is conditionally independent of X_b given all the vectors corresponding to the remaining nodes, $X_{-ab} = \{X_c : c \in V \setminus \{a, b\}\}$. Such a graph is also known as a Markov network (of Markov graph), which we shall emphasize in this paper to compare with an alternative graph over V known as the association network, which is based on pairwise marginal independence. Conditional independence can be read from the inverse of the covariance matrix, as the block corresponding to X_a and X_b will be equal to zero. Let $\mathcal{D}_n = \{x_i\}_{i=1}^n$ be a sample of n independent and identically distributed vectors drawn from $N(0, \Sigma)$. For a vector x_i , we denote

$x_{i,a} \in \mathbb{R}^{k_a}$ the component corresponding to the node $a \in V$. Our goal is to estimate the structure of the graph G from the sample \mathcal{D}_n . Note that we allow for different nodes to have different number of attributes, which is useful in many applications, e.g., when a node represents a gene pathway in a regulatory network.

Using the standard Gaussian graphical model for univariate nodal observations, one can estimate the Markov graph for each attribute individually by estimating the sparsity pattern of the precision matrix $\Omega = \Sigma^{-1}$. This is also known as the covariance selection problem (Dempster, 1972). For high dimensional problems, Meinshausen and Bühlmann (2006) propose a parallel Lasso approach for estimating Gaussian graphical models by solving a collection of sparse regression problems. This procedure can be viewed as a pseudo-likelihood based method. In contrast, Banerjee et al. (2008), Yuan and Lin (2007), and Friedman et al. (2008) take a penalized likelihood approach to estimate the sparse precision matrix Ω . To reduce estimation bias, Lam and Fan (2009), Johnson et al. (2012), and Shen et al. (2012) developed the non-concave penalties to penalize the likelihood function. More recently, Yuan (2010) and Cai et al. (2011) proposed the graphical Dantzig selector and CLIME, which can be solved by linear programming and are more amenable to theoretical analysis than the penalized likelihood approach. Under certain regularity conditions, these methods have proven to be graph estimation consistent (Ravikumar et al., 2011, Yuan, 2010, Cai et al., 2011) and scalable software packages, such as glasso and huge, were developed to implement these algorithms (Zhao et al., 2012). However, in the case of multi-attribute data, it is not clear how to combine estimated graphs to obtain a single Markov graph reflecting the structure of the underlying complex system. This is especially the case when nodes in the graph contain different number of attributes.

In a previous work, Katenka and Kolaczyk (2011) proposed a method for estimating association networks from multi-attribute data using canonical correlation as a dependence measure between two groups of attributes. However, association networks are known to confound the direct interactions with indirect ones as they only represent marginal associations. In contrast, we develop a method based on partial canonical correlation, which give rise to a Markov graph that is better suited for separating direct interactions from indirect confounders. Our work is related to the literature on simultaneous estimation of multiple Gaussian graphical models under a multi-task setting (Guo et al., 2011, Varoquaux et al., 2010, Honorio and Samaras, 2010, Chiquet et al., 2011, Danaher et al., 2011). However, the model given in (1) is different from models considered in various multi-task settings and the optimization algorithms developed in the multi-task literature do not extend to handle the optimization problem given in our setting.

Unlike the standard procedures for estimating the structure of Gaussian graphical models (e.g., neighborhood selection (Meinshausen and Bühlmann, 2006) or glasso (Friedman et al., 2008)), which infer the partial correlations between pairs of multi-attribute nodes, our proposed method estimates the partial canonical correlations between pairs of nodes, which leads to a graph estimator over multi-attribute nodes that bears the same probabilistic independence interpretations as that of the graph from

Gaussian graphical model over univariate nodes. Under this new framework, the contributions of this paper include: (i) Computationally, an efficient algorithm is provided to estimate the multi-attribute Markov graphs; (ii) Theoretically, we provide sufficient conditions which guarantee consistent graph recovery; and (iii) Empirically, we apply our procedure to uncover gene regulatory networks from gene and protein profiles, and to uncover brain connectivity graph from functional magnetic resonance imaging data.

2 Methodology

In this section, we propose to estimate the graph by estimating non-zero partial canonical correlation between the nodes. This leads to a penalized maximum likelihood objective, for which we develop an efficient optimization procedure.

2.1 Preliminaries

Let X_a and X_b be two multivariate random vectors. Canonical correlation is defined between X_a and X_b as

$$\rho_c(X_a, X_b) = \max_{u \in \mathbb{R}^{k_a}, v \in \mathbb{R}^{k_b}} \text{corr}(u^T X_a, v^T X_b).$$

That is, computing canonical correlation between X_a and X_b is equivalent to maximizing the correlation between two linear combinations $u^T X_a$ and $v^T X_b$ with respect to vectors u and v . Canonical correlation can be used to measure association strength between two nodes with multi-attribute observations. For example, in Katenka and Kolaczyk (2011), a graph is estimated from multi-attribute nodal observations by elementwise thresholding the canonical correlation matrix between nodes, but such a graph estimator may confound the direct interactions with indirect ones.

In this paper, we exploit the partial canonical correlation to estimate a graph from multi-attribute nodal observations. A graph is going to be formed by connecting nodes with non-zero partial canonical correlation. Let $\hat{A} = \text{argmin}_E (\|X_a - AX_{-ab}\|_2^2)$ and $\hat{B} = \text{argmin}_E (\|X_b - BX_{-ab}\|_2^2)$, then the partial canonical correlation between X_a and X_b is defined as

$$\rho_c(X_a, X_b; X_{-ab}) = \max_{u \in \mathbb{R}^{k_a}, v \in \mathbb{R}^{k_b}} \text{corr}\{u^T(X_a - \hat{A}X_{-ab}), v^T(X_b - \hat{B}X_{-ab})\}, \quad (2)$$

that is, the partial canonical correlation between X_a and X_b is equal to the canonical correlation between the residual vectors of X_a and X_b after the effect of X_{-ab} is removed (Rao, 1969).

Let Ω^* denote the precision matrix under the model in (1). Using standard results for the multivariate Gaussian distribution (see also Equation (7) in Rao (1969)), a straightforward calculation shows that¹

$$\rho_c(X_a, X_b; X_{-ab}) \neq 0 \quad \text{if and only if} \quad \max_{u \in \mathbb{R}^{k_a}, v \in \mathbb{R}^{k_b}} u^T \Omega_{ab}^* v \neq 0. \quad (3)$$

¹Calculation given in Appendix C.3

This implies that estimating whether the partial canonical correlation is zero or not can be done by estimating whether a block of the precision matrix is zero or not. Furthermore, under the model in (1), vectors X_a and X_b are conditionally independent given X_{-ab} if and only if partial canonical correlation is zero. A graph built on this type of inter-nodal relationship is known as a Markov graph, as it captures both local and global Markov properties over all arbitrary subsets of nodes in the graph, even though the graph is built based on pairwise conditional independence properties. In §2.2, we use the above observations to design an algorithm that estimates the non-zero partial canonical correlation between nodes from data \mathcal{D}_n using the penalized maximum likelihood estimation of the precision matrix.

Based on the relationship given in (3), we can motivate an alternative method for estimating the non-zero partial canonical correlation. Let $\bar{a} = \{b : b \in V \setminus \{a\}\}$ denote the set of all nodes minus the node a . Then

$$E(X_a | X_{\bar{a}} = x_{\bar{a}}) = \Sigma_{a,\bar{a}}^* \Sigma_{\bar{a},\bar{a}}^{*,-1} x_{\bar{a}}.$$

Since $\Omega_{a,\bar{a}}^* = -(\Sigma_{aa}^* - \Sigma_{a,\bar{a}}^* \Sigma_{\bar{a},\bar{a}}^{*,-1} \Sigma_{\bar{a},a}^*)^{-1} \Sigma_{a,\bar{a}}^* \Sigma_{\bar{a},\bar{a}}^{*,-1}$, we observe that a zero block Ω_{ab} can be identified from the regression coefficients when each component of X_a is regressed on $X_{\bar{a}}$. We do not build an estimation procedure around this observation, however, we note that this relationship shows how one would develop a regression based analogue of the work presented in Katenka and Kolaczyk (2011).

2.2 Penalized Log-Likelihood Optimization

Based on the data \mathcal{D}_n , we propose to minimize the penalized negative Gaussian log-likelihood under the model in (1),

$$\min_{\Omega > 0} \left\{ \text{tr } S\Omega - \log |\Omega| + \lambda \sum_{a,b} \|\Omega_{ab}\|_F \right\} \quad (4)$$

where $S = n^{-1} \sum_{i=1}^n x_i x_i^T$ is the sample covariance matrix, $\|\Omega_{ab}\|_F$ denotes the Frobenius norm of Ω_{ab} and λ is a user defined parameter that controls the sparsity of the solution $\hat{\Omega}$. The Frobenius norm penalty encourages blocks of the precision matrix to be equal to zero, similar to the way that the ℓ_2 penalty is used in the group Lasso (Yuan and Lin, 2006). Here we assume that the same number of samples is available per attribute. However, the same method can be used in cases when some samples are obtained on a subset of attributes. Indeed, we can simply estimate each element of the matrix S from available samples, treating non-measured attributes as missing completely at random (for more details see Kolar and Xing, 2012).

The dual problem to (4) is

$$\max_{\Sigma} \sum_{j \in V} k_j + \log |\Sigma| \quad \text{subject to} \quad \max_{a,b} \|S_{ab} - \Sigma_{ab}\|_F \leq \lambda, \quad (5)$$

where Σ is the dual variable to Ω and $|\Sigma|$ denotes the determinant of Σ . Note that the primal problem gives us an estimate of the precision matrix, while the dual problem

estimates the covariance matrix. The proposed optimization procedure, described below, will simultaneously estimate the precision matrix and covariance matrix, without explicitly performing an expensive matrix inversion.

We propose to optimize the objective function in (4) using an inexact block coordinate descent procedure, inspired by Mazumder and Agarwal (2011). The block coordinate descent is an iterative procedure that operates on a block of rows and columns while keeping the other rows and columns fixed. We write

$$\Omega = \begin{pmatrix} \Omega_{aa} & \Omega_{a,\bar{a}} \\ \Omega_{\bar{a},a} & \Omega_{\bar{a},\bar{a}} \end{pmatrix}, \quad \Sigma = \begin{pmatrix} \Sigma_{aa} & \Sigma_{a,\bar{a}} \\ \Sigma_{\bar{a},a} & \Sigma_{\bar{a},\bar{a}} \end{pmatrix}, \quad S = \begin{pmatrix} S_{aa} & S_{a,\bar{a}} \\ S_{\bar{a},a} & S_{\bar{a},\bar{a}} \end{pmatrix}$$

and suppose that $(\tilde{\Omega}, \tilde{\Sigma})$ are the current estimates of the precision matrix and covariance matrix. With the above block partition, we have $\log |\Omega| = \log(\Omega_{\bar{a},\bar{a}}) + \log(\Omega_{aa} - \Omega_{a,\bar{a}}(\Omega_{\bar{a},\bar{a}})^{-1}\Omega_{\bar{a},a})$. In the next iteration, $\hat{\Omega}$ is of the form

$$\hat{\Omega} = \tilde{\Omega} + \begin{pmatrix} \Delta_{aa} & \Delta_{a,\bar{a}} \\ \Delta_{\bar{a},a} & 0 \end{pmatrix} = \begin{pmatrix} \hat{\Omega}_{aa} & \hat{\Omega}_{a,\bar{a}} \\ \hat{\Omega}_{\bar{a},a} & \hat{\Omega}_{\bar{a},\bar{a}} \end{pmatrix}$$

and is obtained by minimizing

$$\text{tr } S_{aa}\Omega_{aa} + 2 \text{tr } S_{a,\bar{a}}\Omega_{\bar{a},a} - \log |\Omega_{aa} - \Omega_{a,\bar{a}}(\tilde{\Omega}_{\bar{a},\bar{a}})^{-1}\Omega_{\bar{a},a}| + \lambda \|\Omega_{aa}\|_F + 2\lambda \sum_{b \neq a} \|\Omega_{ab}\|_F. \quad (6)$$

Exact minimization over the variables Ω_{aa} and $\Omega_{a,\bar{a}}$ at each iteration of the block coordinate descent procedure can be computationally expensive. Therefore, we propose to update Ω_{aa} and $\Omega_{a,\bar{a}}$ using one generalized gradient step update (see Beck and Teboulle (2009)) in each iteration. Note that the objective function in (6) is a sum of a smooth convex function and a non-smooth convex penalty so that the gradient descent method cannot be directly applied. Given a step size t , generalized gradient descent optimizes a quadratic approximation of the objective at the current iterate $\tilde{\Omega}$, which results in the following two updates

$$\hat{\Omega}_{aa} = \underset{\Omega_{aa}}{\text{argmin}} \left\{ \text{tr}(S_{aa} - \tilde{\Sigma}_{aa})\Omega_{aa} + \frac{1}{2t} \|\Omega_{aa} - \tilde{\Omega}_{aa}\|_F^2 + \lambda \|\Omega_{aa}\|_F \right\}, \quad \text{and} \quad (7)$$

$$\hat{\Omega}_{ab} = \underset{\Omega_{ab}}{\text{argmin}} \left\{ \text{tr}(S_{ab} - \tilde{\Sigma}_{ab})\Omega_{ba} + \frac{1}{2t} \|\Omega_{ab} - \tilde{\Omega}_{ab}\|_F^2 + \lambda \|\Omega_{ab}\|_F \right\}, \quad \forall b \in \bar{a}. \quad (8)$$

If the resulting estimator $\hat{\Omega}$ is not positive definite or the update does not decrease the objective, we halve the step size t and find a new update. Once the update of the precision matrix $\hat{\Omega}$ is obtained, we update the covariance matrix $\hat{\Sigma}$. Updates to the precision and covariance matrices can be found efficiently, without performing expensive matrix inversion, as we show in Appendix A (see (11)–(13)). Combining all three steps we get the following algorithm:

1. Set the initial estimator $\tilde{\Omega} = \text{diag}(S)$ and $\tilde{\Sigma} = \tilde{\Omega}^{-1}$. Set the step size $t = 1$.

2. For each $a \in V$ perform the following:

Update $\hat{\Omega}$ using (11) and (12).

If $\hat{\Omega}$ is not positive definite, set $t \leftarrow t/2$ and repeat the update.

Update $\hat{\Sigma}$ using (13).

3. Repeat Step 2 until the duality gap

$$\left| \text{tr}(S\hat{\Omega}) - \log |\hat{\Omega}| + \lambda \sum_{a,b} \|\hat{\Omega}_{ab}\|_F - \sum_{j \in V} k_j - \log |\Sigma| \right| \leq \epsilon,$$

where ϵ is a prefixed precision parameter (for example, $\epsilon = 10^{-3}$).

Finally, we form a graph $\hat{G} = (V, \hat{E})$ by connecting nodes with $\|\hat{\Omega}_{ab}\|_F \neq 0$.

Computational complexity of the procedure is given in Appendix B. Convergence of the above described procedure to the unique minimum of the objective function in (4) does not follow from the standard results on the block coordinate descent algorithm (Tseng, 2001) for two reasons. First, the minimization problem in (6) is not solved exactly at each iteration, since we only update Ω_{aa} and $\Omega_{a,\bar{a}}$ using one generalized gradient step update in each iteration. Second, the blocks of variables, over which the optimization is done at each iteration, are not completely separable between iterations due to the symmetry of the problem. The proof of the following convergence result is given in Appendix C.

Lemma 1. *For every value of $\lambda > 0$, the above described algorithm produces a sequence of estimates $\{\tilde{\Omega}^{(t)}\}_{t \geq 1}$ of the precision matrix that monotonically decrease the objective values given in (4). Every element of this sequence is positive definite and the sequence converges to the unique minimizer $\hat{\Omega}$ of (4).*

2.3 Efficient Identification of Connected Components

When the target graph \hat{G} is composed of smaller, disconnected components, the solution to the problem in (4) is block diagonal (possibly after permuting the node indices) and can be obtained by solving smaller optimization problems. That is, the minimizer $\hat{\Omega}$ can be obtained by solving (4) for each connected component independently, resulting in massive computational gains. We give necessary and sufficient condition for the solution $\hat{\Omega}$ of (4) to be block-diagonal, which can be easily checked by inspecting the empirical covariance matrix S .

Our first result follows immediately from the Karush-Kuhn-Tucker conditions for the optimization problem (4) and states that if $\hat{\Omega}$ is block-diagonal, then it can be obtained by solving a sequence of smaller optimization problems.

Lemma 2. *If the solution to (4) takes the form $\hat{\Omega} = \text{diag}(\hat{\Omega}_1, \hat{\Omega}_2, \dots, \hat{\Omega}_l)$, that is, $\hat{\Omega}$ is a block diagonal matrix with the diagonal blocks $\hat{\Omega}_1, \dots, \hat{\Omega}_l$, then it can be obtained by solving*

$$\min_{\Omega_{l'} > 0} \left\{ \text{tr} S_{l'} \Omega_{l'} - \log |\Omega_{l'}| + \lambda \sum_{a,b} \|\Omega_{ab}\|_F \right\}$$

separately for each $l' = 1, \dots, l$, where $S_{l'}$ are submatrices of S corresponding to $\Omega_{l'}$.

Next, we describe how to identify diagonal blocks of $\hat{\Omega}$. Let $\mathcal{P} = \{P_1, P_2, \dots, P_l\}$ be a partition of the set V and assume that the nodes of the graph are ordered in a way that if $a \in P_j, b \in P_{j'}, j < j'$, then $a < b$. The following lemma states that the blocks of $\hat{\Omega}$ can be obtained from the blocks of a thresholded sample covariance matrix.

Lemma 3. *A necessary and sufficient conditions for $\hat{\Omega}$ to be block diagonal with blocks P_1, P_2, \dots, P_l is that $\|S_{ab}\|_F \leq \lambda$ for all $a \in P_j, b \in P_{j'}, j \neq j'$.*

Blocks P_1, P_2, \dots, P_l can be identified by forming a $p \times p$ matrix Q with elements $q_{ab} = \mathbb{I}\{\|S_{ab}\|_F > \lambda\}$ and computing connected components of the graph with adjacency matrix Q . The lemma states also that given two penalty parameters $\lambda_1 < \lambda_2$, the set of unconnected nodes with penalty parameter λ_1 is a subset of unconnected nodes with penalty parameter λ_2 . The simple check above allows us to estimate graphs on datasets with large number of nodes, if we are interested in graphs with small number of edges. However, this is often the case when the graphs are used for exploration and interpretation of complex systems. Lemma 3 is related to existing results established for speeding-up computation when learning single and multiple Gaussian graphical models (Witten et al., 2011, Mazumder and Hastie, 2012, Danaher et al., 2011). Each condition is different, since the methods optimize different objective functions.

3 Consistent Graph Identification

In this section, we provide theoretical analysis of the estimator described in §2.2. In particular, we provide sufficient conditions for consistent graph recovery. For simplicity of presentation, we assume that $k_a = k$, for all $a \in V$, that is, we assume that the same number of attributes is observed for each node. For each $a = 1, \dots, kp$, we assume that $(\sigma_{aa}^*)^{-1/2} X_a$ is sub-Gaussian with parameter γ , where σ_{aa}^* is the a th diagonal element of Σ^* . Recall that Z is a sub-Gaussian random variable if there exists a constant $\sigma \in (0, \infty)$ such that

$$E(\exp(tZ)) \leq \exp(\sigma^2 t^2), \text{ for all } t \in \mathbb{R}.$$

Our assumptions involve the Hessian of the function $f(A) = \text{tr} SA - \log |A|$ evaluated at the true Ω^* , $\mathcal{H} = \mathcal{H}(\Omega^*) = (\Omega^*)^{-1} \otimes (\Omega^*)^{-1} \in \mathbb{R}^{(pk)^2 \times (pk)^2}$, with \otimes denoting the Kronecker product, and the true covariance matrix Σ^* . The Hessian and the covariance matrix can be thought of as block matrices with blocks of size $k^2 \times k^2$ and $k \times k$, respectively. We will make use of the operator $\mathcal{C}(\cdot)$ that operates on these block matrices and outputs a smaller matrix with elements that equal to the Frobenius norm of the original blocks. For example, $\mathcal{C}(\Sigma^*) \in \mathbb{R}^{p \times p}$ with elements $\mathcal{C}(\Sigma^*)_{ab} = \|\Sigma_{ab}^*\|_F$. Let $\mathcal{T} = \{(a, b) : \|\Omega_{ab}\|_F \neq 0\}$ and $\mathcal{N} = \{(a, b) : \|\Omega_{ab}\|_F = 0\}$. With this notation introduced, we assume that the following irrerepresentable condition holds. There exists a constant $\alpha \in [0, 1)$ such that

$$\|\mathcal{C}(\mathcal{H}_{\mathcal{N}\mathcal{T}}(\mathcal{H}_{\mathcal{T}\mathcal{T}})^{-1})\|_\infty \leq 1 - \alpha, \tag{9}$$

where $\|A\|_\infty = \max_i \sum_j |A_{ij}|$. We will also need the following quantities to specify the results $\kappa_{\Sigma^*} = \|\mathcal{C}(\Sigma^*)\|_\infty$ and $\kappa_{\mathcal{H}} = \|\mathcal{C}(\mathcal{H}_{\mathcal{T}\mathcal{T}}^{-1})\|_\infty$. These conditions extend the conditions specified in Ravikumar et al. (2011) needed for estimating graphs from single attribute observations.

We have the following result that provides sufficient conditions for the exact recovery of the graph.

Proposition 4. *Let $\tau > 2$. We set the penalty parameter λ in (4) as*

$$\lambda = 8k\alpha^{-1} \left(128(1 + 4\gamma^2)^2 (\max_a \sigma_{aa}^*)^2 n^{-1} (2 \log(2k) + \tau \log(p)) \right)^{1/2}.$$

If $n > C_1 s^2 k^2 (1 + 8\alpha^{-1})^2 (\tau \log p + \log 4 + 2 \log k)$, where s is the maximal degree of nodes in G , $C_1 = (48\sqrt{2}(1 + 4\gamma^2) (\max_a \sigma_{aa}^) \max(\kappa_{\Sigma^*} \kappa_{\mathcal{H}}, \kappa_{\Sigma^*}^3 \kappa_{\mathcal{H}}^2))^2$ and*

$$\min_{(a,b) \in \mathcal{T}, a \neq b} \|\Omega_{ab}\|_F > 16\sqrt{2}(1+4\gamma^2) (\max_a \sigma_{aa}^*) (1+8\alpha^{-1}) \kappa_{\mathcal{H}} k \left(\frac{\tau \log p + \log 4 + 2 \log k}{n} \right)^{1/2},$$

then $\text{pr}(\hat{G} = G) \geq 1 - p^{2-\tau}$.

The proof of Proposition 4 is given in Appendix C. We extend the proof of Ravikumar et al. (2011) to accommodate the Frobenius norm penalty on blocks of the precision matrix. This proposition specifies the sufficient sample size and a lower bound on the Frobenius norm of the off-diagonal blocks needed for recovery of the unknown graph. Under these conditions and correctly specified tuning parameter λ , the solution to the optimization problem in (4) correctly recovers the graph with high probability. In practice, one needs to choose the tuning parameter in a data dependent way. For example, using the Bayesian information criterion. Even though our theoretical analysis obtains the same rate of convergence as that of Ravikumar et al. (2011), our method has a significantly improved finite-sample performance (More details will be provided in §5.). It remains an open question whether the sample size requirement can be improved as in the case of group Lasso (see, for example, Lounici et al., 2011). The analysis of Lounici et al. (2011) relies heavily on the special structure of the least squares regression. Hence, their method does not carry over to the more complicated objective function as in (4).

4 Interpreting Edges

We propose a post-processing step that will allow us to quantify the strength of links identified by the method proposed in §2.2, as well as identify important attributes that contribute to the existence of links.

For any two nodes a and b for which $\Omega_{ab} \neq 0$, we define $\mathcal{N}(a, b) = \{c \in V \setminus \{a, b\} : \Omega_{ac} \neq 0 \text{ or } \Omega_{bc} \neq 0\}$, which is the Markov blanket for the set of nodes $\{X_a, X_b\}$. Note that the conditional distribution of $(X_a^T, X_b^T)^T$ given $X_{-\{a,b\}}$ is equal to the conditional

distribution of $(X_a^T, X_b^T)^T$ given $X_{\mathcal{N}(a,b)}$. Now,

$$\begin{aligned}\rho_c(X_a, X_b; X_{-ab}) &= \rho_c(X_a, X_b; X_{\mathcal{N}(a,b)}) \\ &= \max_{w_a \in \mathbb{R}^{k_a}, w_b \in \mathbb{R}^{k_b}} \text{corr}(u^T(X_a - \tilde{A}X_{\mathcal{N}(a,b)}), v^T(X_b - \tilde{B}X_{\mathcal{N}(a,b)})),\end{aligned}$$

where $\tilde{A} = \text{argmin } E(\|X_a - AX_{\mathcal{N}(a,b)}\|_2^2)$ and $\tilde{B} = \text{argmin } E(\|X_b - BX_{\mathcal{N}(a,b)}\|_2^2)$. Let $\bar{\Sigma}(a, b) = \text{var}(X_a, X_b \mid X_{\mathcal{N}(a,b)})$. Now we can express the partial canonical correlation as

$$\rho_c(X_a, X_b; X_{\mathcal{N}(a,b)}) = \max_{w_a \in \mathbb{R}^{k_a}, w_b \in \mathbb{R}^{k_b}} \frac{w_a^T \bar{\Sigma}_{ab} w_b}{(w_a^T \bar{\Sigma}_{aa} w_a)^{1/2} (w_b^T \bar{\Sigma}_{bb} w_b)^{1/2}}$$

where

$$\bar{\Sigma}(a, b) = \begin{pmatrix} \bar{\Sigma}_{aa} & \bar{\Sigma}_{ab} \\ \bar{\Sigma}_{ba} & \bar{\Sigma}_{bb} \end{pmatrix}.$$

The weight vectors w_a and w_b can be easily found by solving the system of eigenvalue equations

$$\begin{cases} \bar{\Sigma}_{aa}^{-1} \bar{\Sigma}_{ab} \bar{\Sigma}_{bb}^{-1} \bar{\Sigma}_{ba} w_a = \phi^2 w_a \\ \bar{\Sigma}_{bb}^{-1} \bar{\Sigma}_{ba} \bar{\Sigma}_{aa}^{-1} \bar{\Sigma}_{ab} w_b = \phi^2 w_b \end{cases} \quad (10)$$

with w_a and w_b being the vectors that correspond to the maximum eigenvalue ϕ^2 . Furthermore, we have $\rho_c(X_a, X_b; X_{\mathcal{N}(a,b)}) = \phi$. Following Katenka and Kolaczyk (2011), the weights w_a, w_b can be used to access the relative contribution of each attribute to the edge between the nodes a and b . In particular, the weight $(w_{a,i})^2$ characterizes the relative contribution of the i th attribute of node a to $\rho_c(X_a, X_b; X_{\mathcal{N}(a,b)})$.

Given an estimate $\hat{\mathcal{N}}(a, b) = \{c \in V \setminus \{a, b\} : \hat{\Omega}_{ac} \neq 0 \text{ or } \hat{\Omega}_{bc} \neq 0\}$ of the Markov blanket $\mathcal{N}(a, b)$, we form the residual vectors

$$r_{i,a} = x_{i,a} - \check{A}x_{i,\hat{\mathcal{N}}(a,b)}, \quad r_{i,b} = x_{i,b} - \check{B}x_{i,\hat{\mathcal{N}}(a,b)},$$

where \check{A} and \check{B} are the least square estimators of \tilde{A} and \tilde{B} . Given the residuals, we form $\check{\Sigma}(a, b)$, the empirical version of the matrix $\bar{\Sigma}(a, b)$, by setting

$$\check{\Sigma}_{aa} = \text{corr}(\{r_{i,a}\}_{i \in [n]}), \quad \check{\Sigma}_{bb} = \text{corr}(\{r_{i,b}\}_{i \in [n]}), \quad \check{\Sigma}_{ab} = \text{corr}(\{r_{i,a}\}_{i \in [n]}, \{r_{i,b}\}_{i \in [n]}).$$

Now, solving the eigenvalue system in (10) will give us estimates of the vectors w_a, w_b and the partial canonical correlation.

Note that we have described a way to interpret the elements of the off-diagonal blocks in the estimated precision matrix. The elements of the diagonal blocks, which correspond to coefficients between attributes of the same node, can still be interpreted by their relationship to the partial correlation coefficients.

5 Simulation Studies

In this section, we perform a set of simulation studies to illustrate finite sample performance of our method. We demonstrate that the scalings of (n, p, s) predicted by the theory are sharp. Furthermore, we compare against three other methods: 1) a method that uses the glasso first to estimate one graph over each of the k individual attributes and then creates an edge in the resulting graph if an edge appears in at least one of the single attribute graphs, 2) the method of Guo et al. (2011) and 3) the method of Danaher et al. (2011). We have also tried applying the glasso to estimate the precision matrix for the model in (1) and then post-processing it, so that an edge appears in the resulting graph if the corresponding block of the estimated precision matrix is non-zero. The result of this method is worse compared to the first baseline, so we do not report it here.

All the methods above require setting one or two tuning parameters that control the sparsity of the estimated graph. We select these tuning parameters by minimizing the Bayesian information criterion, which balances the goodness of fit of the model and its complexity, over a grid of parameter values. For our multi-attribute method, the Bayesian information criterion takes the following form

$$\text{BIC}(\lambda) = \text{tr}(S\hat{\Omega}) - \log |\hat{\Omega}| + \sum_{a < b} \mathbb{I}\{\hat{\Omega}_{ab} \neq 0\} k_a k_b \log(n).$$

Other methods for selecting tuning parameters are possible, like minimization of cross-validation or Akaike information criterion. However, these methods tend to select models that are too dense.

Theoretical results given in §3 characterize the sample size needed for consistent recovery of the underlying graph. In particular, Proposition 4 suggests that we need $n = \theta s^2 k^2 \log(pk)$ samples to estimate the graph structure consistently, for some $\theta > 0$. Therefore, if we plot the hamming distance between the true and recovered graph against θ , we expect the curves to reach zero distance for different problem sizes at a same point. We verify this on randomly generated chain and nearest-neighbors graphs.

We generate data as follows. A random graph with p nodes is created by first partitioning nodes into $p/20$ connected components, each with 20 nodes, and then forming a random graph over these 20 nodes. A chain graph is formed by permuting the nodes and connecting them in succession, while a nearest-neighbor graph is constructed following the procedure outlined in Li and Gui (2006). That is, for each node, we draw a point uniformly at random on a unit square and compute the pairwise distances between nodes. Each node is then connected to $s = 4$ closest neighbors. Since some of nodes will have more than 4 adjacent edges, we randomly remove edges from nodes that have degree larger than 4 until the maximum degree of a node in a network is 4. Once the graph is created, we construct a precision matrix, with non-zero blocks corresponding to edges in the graph. Elements of diagonal blocks are set as $0.5^{|a-b|}$, $0 \leq a, b \leq k$, while off-diagonal blocks have elements with the same value, 0.2 for chain graphs and $0.3/k$ for nearest-neighbor networks. Finally, we add ρI to the precision matrix, so that its minimum eigenvalue is equal to 0.5. Note that $s = 2$ for the chain

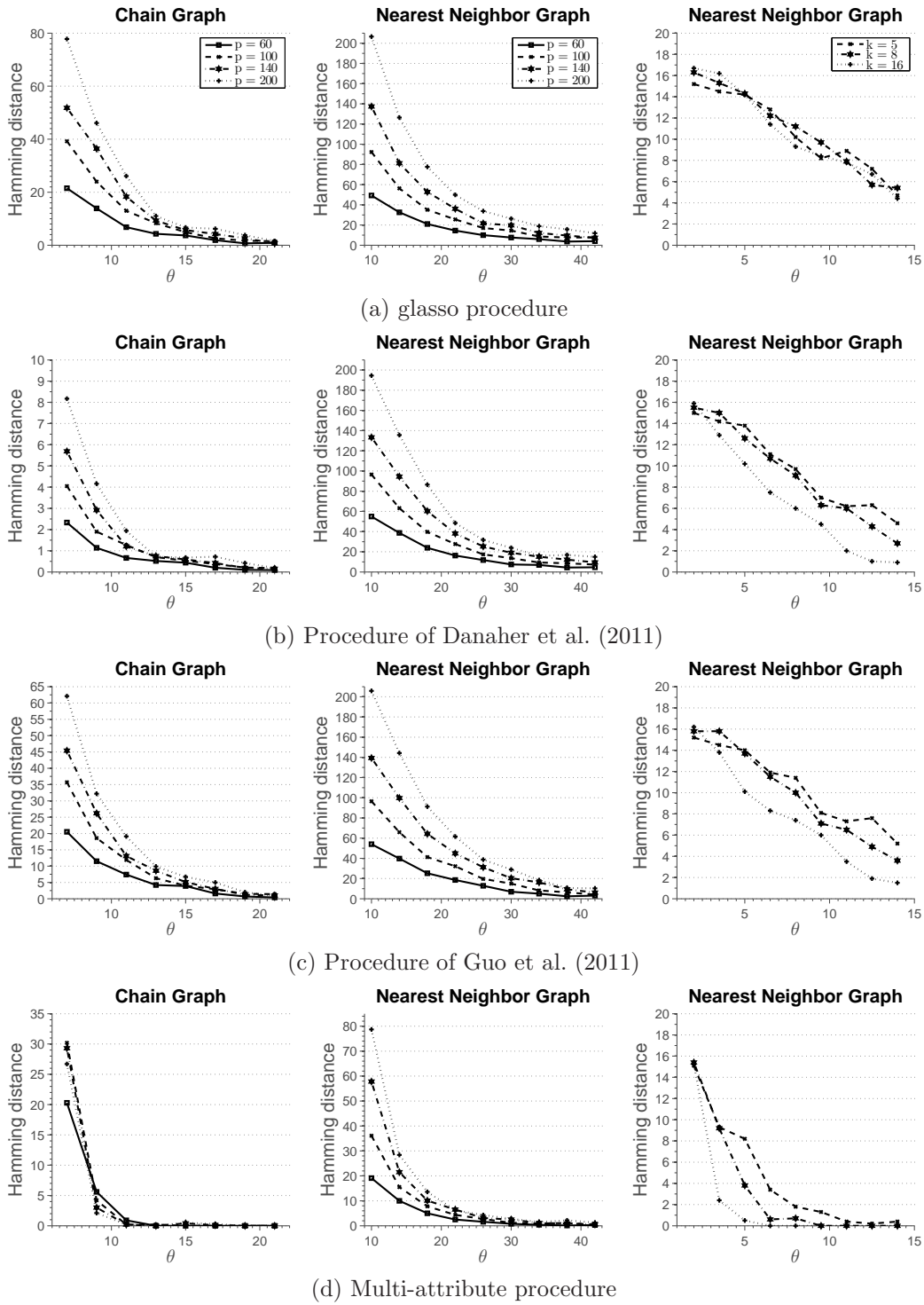


Figure 1: Average hamming distance plotted against the rescaled sample size. Results are averaged over 100 independent runs. Off-diagonal blocks are full matrices.

graph and $s = 4$ for the nearest-neighbor graph. Simulation results are averaged over 100 replicates.

Figure 1 shows simulation results. Each row in the figure reports results for one method, while each column in the figure represents a different simulation setting. For the first two columns, we set $k = 3$ and vary the total number of nodes in the graph. The third simulation setting sets the total number of nodes $p = 20$ and changes the number of attributes k . In the case of the chain graph, we observe that for small sample sizes the method of Danaher et al. (2011) outperforms all the other methods. We note that the multi-attribute method is estimating many more parameters, which require large sample size in order to achieve high accuracy. However, as the sample size increases, we observe that multi-attribute method starts to outperform the other methods. In particular, for the sample size indexed by $\theta = 13$ all the graph are correctly recovered, while other methods fail to recover the graph consistently at the same sample size. In the case of nearest-neighbor graph, none of the methods recover the graph well for small sample sizes. However, for moderate sample sizes, multi-attribute method outperforms the other methods. Furthermore, as the sample size increases none of the other methods recover the graph exactly. This suggests that the conditions for consistent graph recovery may be weaker in the multi-attribute setting.

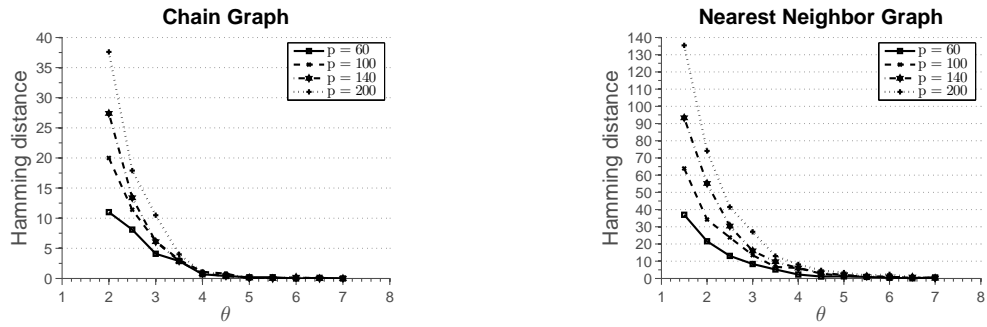
5.1 Alternative Structure of Off-diagonal Blocks

In this section, we investigate performance of different estimation procedures under different assumptions on the elements of the off-diagonal blocks of the precision matrix.

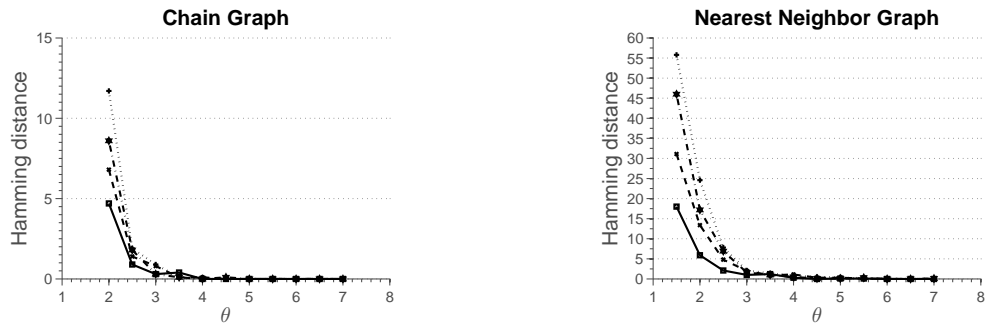
First, we investigate a situation where the multi-attribute method does not perform as well as the methods that estimate multiple graphical models. One such situation arises when different attributes are conditionally independent. To simulate this situation, we use the data generating approach as before, however, we make each block Ω_{ab} of the precision matrix Ω a diagonal matrix. Figure 2 summarizes results of the simulation. We see that the methods of Danaher et al. (2011) and Guo et al. (2011) perform better, since they are estimating much fewer parameters than the multi-attribute method. glasso does not utilize any structural information underlying the estimation problem and requires larger sample size to correctly estimate the graph than other methods.

A completely different situation arises when the edges between nodes can be inferred only based on inter-attribute data, that is, when a graph based on any individual attribute is empty. To generate data under this situation, we follow the procedure as before, but with the diagonal elements of the off-diagonal blocks Ω_{ab} set to zero. Figure 3 summarizes results of the simulation. In this setting, we clearly see the advantage of the multi-attribute method, compared to other three methods. Furthermore, we can see that glasso does better than multi-graph methods of Danaher et al. (2011) and Guo et al. (2011). The reason is that glasso can identify edges based on inter-attribute relationships among nodes, while multi-graph methods rely only on intra-attribute relationships. This simulation illustrates an extreme scenario where inter-attribute relationships are important for identifying edges.

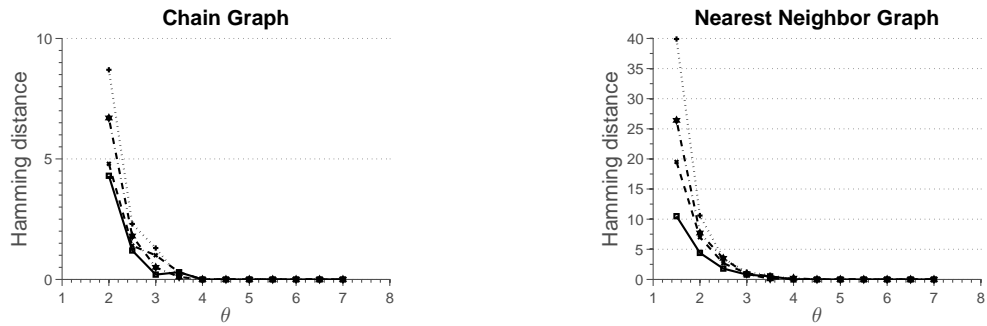
So far, off-diagonal blocks of the precision matrix were constructed to have constant



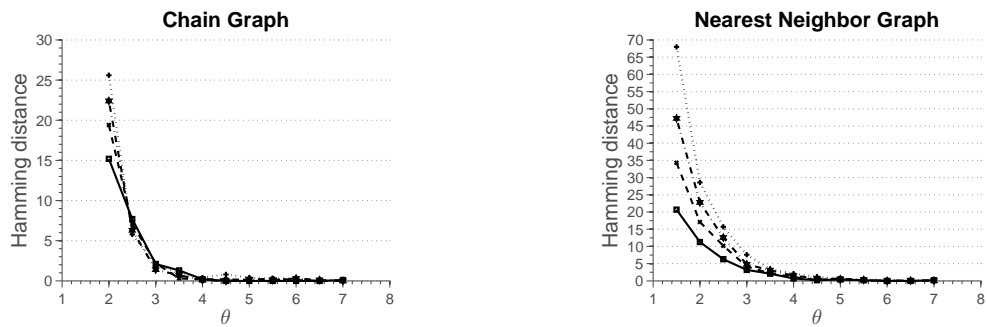
(a) glasso procedure



(b) Procedure of Danaher et al. (2011)

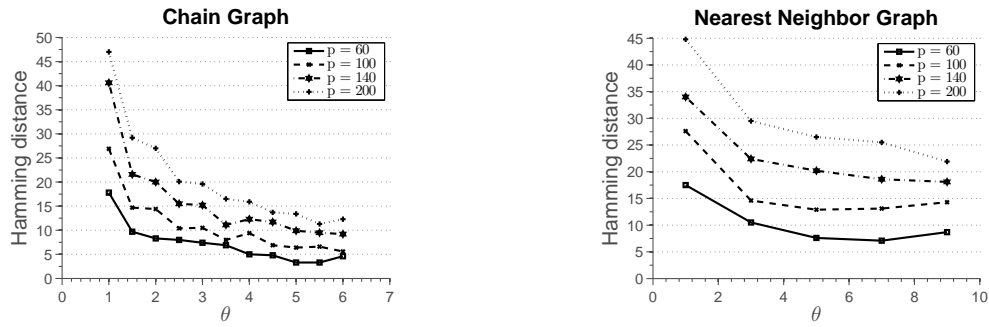


(c) Procedure of Guo et al. (2011)

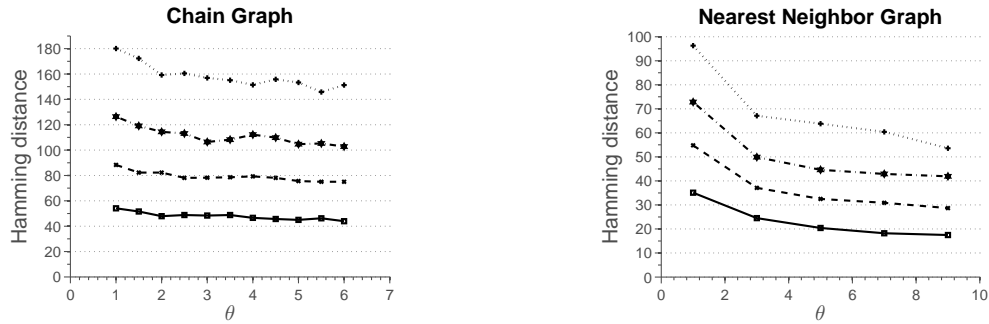


(d) Multi-attribute procedure

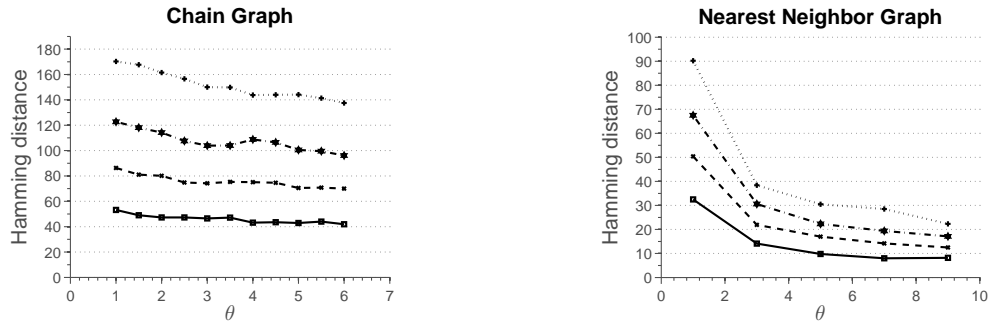
Figure 2: Average hamming distance plotted against the rescaled sample size. Results are averaged over 100 independent runs. Blocks Ω_{ab} of the precision matrix Ω are diagonal matrices.



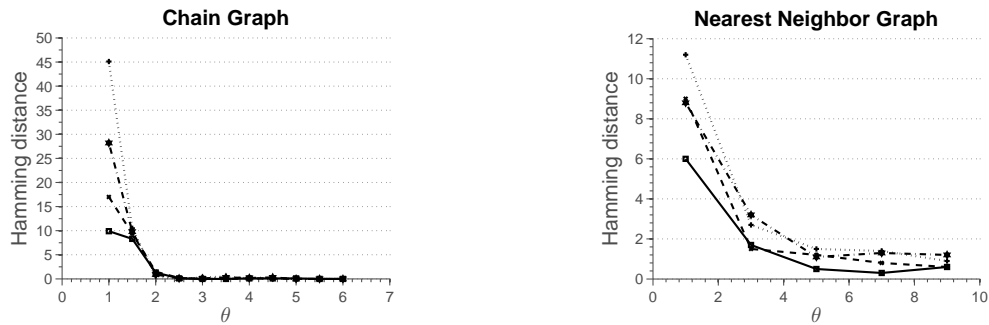
(a) glasso procedure



(b) Procedure of Danaher et al. (2011)

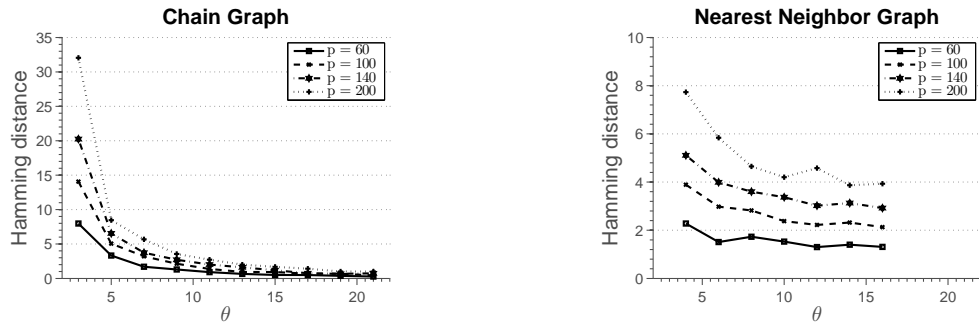


(c) Procedure of Guo et al. (2011)

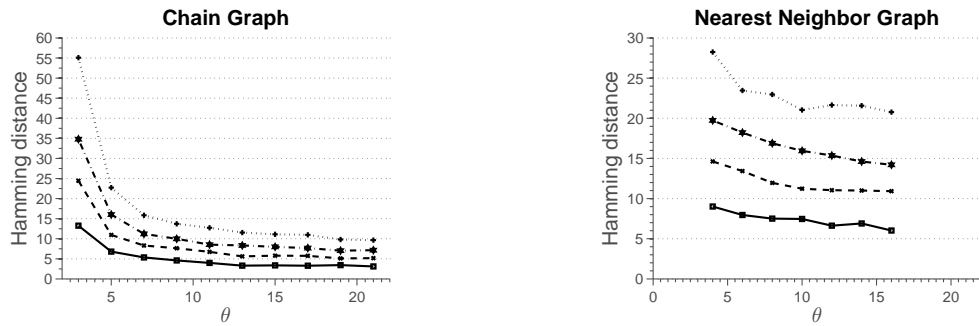


(d) Multi-attribute procedure

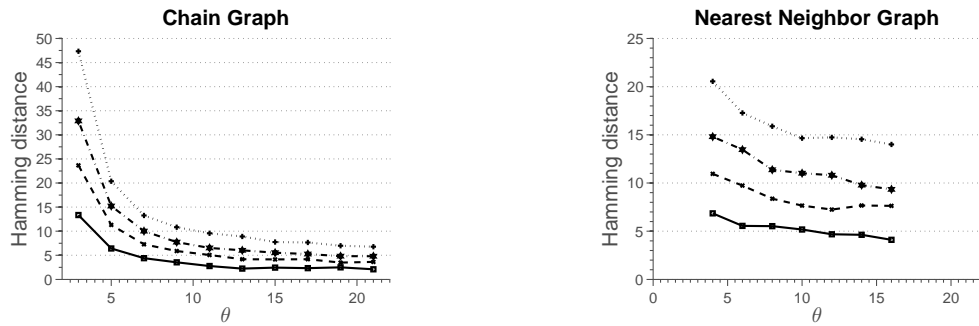
Figure 3: Average hamming distance plotted against the rescaled sample size. Results are averaged over 100 independent runs. Off-diagonal blocks Ω_{ab} of the precision matrix Ω have zeros as diagonal elements.



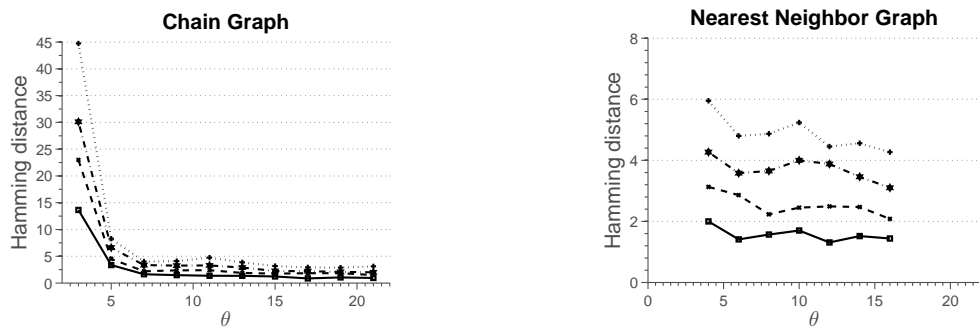
(a) glasso procedure



(b) Procedure of Danaher et al. (2011)



(c) Procedure of Guo et al. (2011)



(d) Multi-attribute procedure

Figure 4: Average hamming distance plotted against the rescaled sample size. Results are averaged over 100 independent runs. Off-diagonal blocks Ω_{ab} of the precision matrix Ω have elements uniformly sampled from $[-0.3, -0.1] \cup [0.1, 0.3]$.

values. Now, we use the same data generating procedure, but generate off-diagonal blocks of a precision matrix in a different way. Each element of the off-diagonal block Ω_{ab} is generated independently and uniformly from the set $[-0.3, -0.1] \cup [0.1, 0.3]$. The results of the simulation are given in Figure 4. Again, qualitatively, the results are similar to those given in Figure 1, except that in this setting more samples are needed to recover the graph correctly.

5.2 Different Number of Samples per Attribute

In this section, we show how to deal with a case when different number of samples is available per attribute. As noted in §2.2, we can treat non-measured attributes as missing completely at random (see Kolar and Xing, 2012, for more details).

Let $R = (r_{il})_{i \in \{1, \dots, n\}, l \in \{1, \dots, pk\}} \in \mathbb{R}^{n \times pk}$ be an indicator matrix, which denotes for each sample point x_i the components that are observed. Then the sample covariance matrix $S = (\sigma_{lk}) \in \mathbb{R}^{pk \times pk}$ is estimated as $\sigma_{lk} = (\sum_{i=1}^n r_{i,l} r_{i,k})^{-1} \sum_{i=1}^n r_{i,l} r_{i,k} x_{i,l} x_{i,k}$. This estimate is plugged into the objective in (4).

We generate a chain graph with $p = 60$ nodes, construct a precision matrix associated with the graph and $k = 3$ attributes, and generate $n = \theta s^2 k^2 \log(pk)$ samples, $\theta > 0$. Next, we generate additional 10%, 30% and 50% samples from the same model, but record only the values for the first attribute. Results of the simulation are given in Figure 5. Qualitatively, the results are similar to those presented in Figure 1.

6 Illustrative Applications to Real Data

In this section, we illustrate how to apply our method to data arising in studies of biological regulatory networks and Alzheimer’s disease.

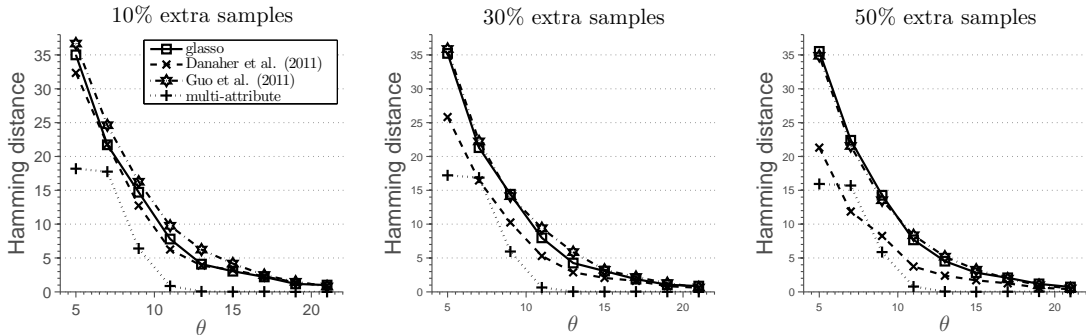


Figure 5: Average hamming distance plotted against the rescaled sample size. Results are averaged over 100 independent runs. Additional samples available for the first attribute.

6.1 Analysis of a Gene/Protein Regulatory Network

We provide illustrative, exploratory analysis of data from the well-known NCI-60 database, which contains different molecular profiles on a panel of 60 diverse human cancer cell lines. Data set consists of protein profiles (normalized reverse-phase lysate arrays for 92 antibodies) and gene profiles (normalized RNA microarray intensities from Human Genome U95 Affymetrix chip-set for > 9000 genes). We focus our analysis on a subset of 91 genes/proteins for which both types of profiles are available. These profiles are available across the same set of 60 cancer cells. More detailed description of the data set can be found in Katenka and Kolaczyk (2011).

We inferred three types of networks: a network based on protein measurements alone, a network based on gene expression profiles and a single gene/protein network. For protein and gene networks we use the `glasso`, while for the gene/protein network, we use our procedure outlined in §2.2. We use the stability selection (Meinshausen and Bühlmann, 2010) procedure to estimate stable networks. In particular, we first select the penalty parameter λ using cross-validation, which over-selects the number of edges in a network. Next, we use the selected λ to estimate 100 networks based on random subsamples containing 80% of the data-points. Final network is composed of stable edges that appear in at least 95 of the estimated networks. Table 1 provides a few summary statistics for the estimated networks. Furthermore, protein and gene/protein networks share 96 edges, while gene and gene/protein networks share 104 edges. Gene and protein network share only 17 edges. Finally, 66 edges are unique to gene/protein network. Figure 6 shows node degree distributions for the three networks. We observe that the estimated networks are much sparser than the association networks in Katenka and Kolaczyk (2011), as expected due to marginal correlations between a number of nodes. The differences in networks require a closer biological inspection by a domain scientist.

We proceed with a further exploratory analysis of the gene/protein network. We investigate the contribution of two nodal attributes to the existence of an edges between the nodes. Following Katenka and Kolaczyk (2011), we use a simple heuristic based on the weight vectors to classify the nodes and edges into three classes. For an edge between the nodes a and b , we take one weight vector, say w_a , and normalize it to have unit norm. Denote w_p the component corresponding to the protein attribute. Left plot in Figure 7 shows the values of w_p^2 over all edges. The edges can be classified into three classes based on the value of w_p^2 . Given a threshold T , the edges for which $w_p^2 \in (0, T)$

Table 1: Summary statistics for protein, gene, and gene/protein networks ($p = 91$).

	protein network	gene network	gene/protein network
Number of edges	122	214	249
Density	0.03	0.05	0.06
Largest connected component	62	89	82
Avg Node Degree	2.68	4.70	5.47
Avg Clustering Coefficient	0.0008	0.001	0.003

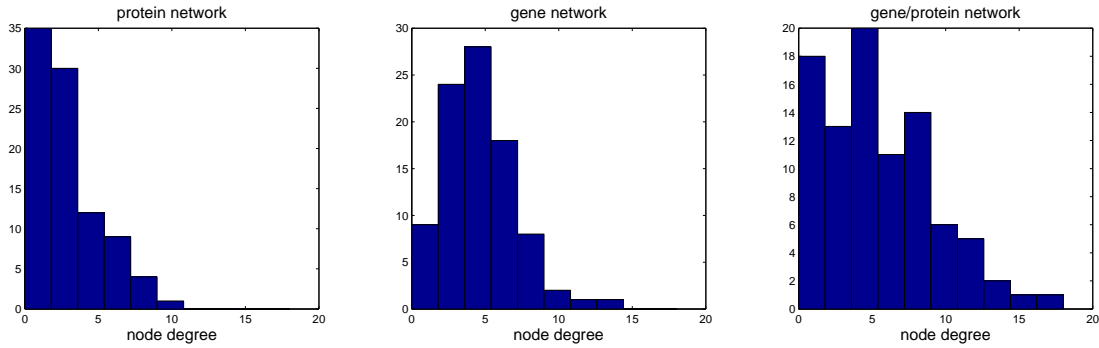


Figure 6: Node degree distributions for protein, gene and gene/protein networks.

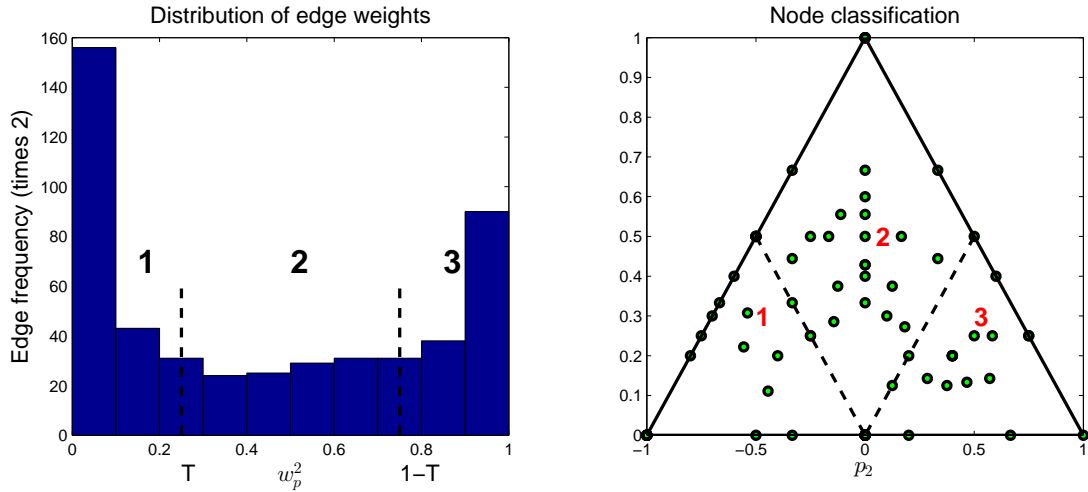


Figure 7: Edge and node classification based on w_p^2 .

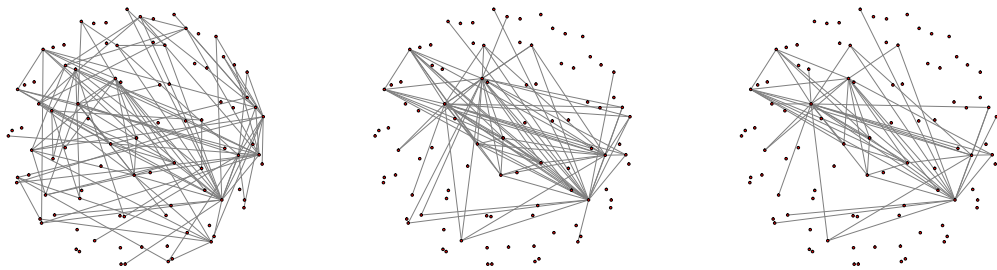
are classified as gene-influenced, the edges for which $w_p^2 \in (1 - T, 1)$ are classified as protein influenced, while the remainder of the edges are classified as mixed type. In the left plot of Figure 7, the threshold is set as $T = 0.25$. Similar classification can be performed for nodes after computing the proportion of incident edges. Let p_1 , p_2 and p_3 denote proportions of gene, protein and mixed edges, respectively, incident with a node. These proportions are represented in a simplex in the right subplot of Figure 7. Nodes with mostly gene edges are located in the lower left corner, while the nodes with mostly protein edges are located in the lower right corner. Mixed nodes are located in the center and towards the top corner of the simplex. Further biological enrichment analysis is possible (see Katenka and Kolaczyk (2011)), however, we do not pursue this here.

6.2 Uncovering Functional Brain Network

We apply our method to the Positron Emission Tomography dataset, which contains 259 subjects, of whom 72 are healthy, 132 have mild cognitive impairment and 55 are diagnosed as Alzheimer’s & Dementia. Note that mild cognitive impairment is a transition stage from normal aging to Alzheimer’s & Dementia. The data can be obtained from <http://adni.loni.ucla.edu/>. The preprocessing is done in the same way as in Huang et al. (2009).

Each Positron Emission Tomography image contains $91 \times 109 \times 91 = 902,629$ voxels. The effective brain region contains 180,502 voxels, which are partitioned into 95 regions, ignoring the regions with fewer than 500 voxels. The largest region contains 5,014 voxels and the smallest region contains 665 voxels. Our preprocessing stage extracts 948 representative voxels from these regions using the K -median clustering algorithm. The parameter K is chosen differently for each region, proportionally to the initial number of voxels in that region. More specifically, for each category of subjects we have an $n \times (d_1 + \dots + d_{95})$ matrix, where n is the number of subjects and $d_1 + \dots + d_{95} = 902,629$ is the number of voxels. Next we set $K_i = \lceil d_i / \sum_j d_j \rceil$, the number of representative voxels in region i , $i = 1, \dots, 95$. The representative voxels are identified by running the K -median clustering algorithm on a sub-matrix of size $n \times d_i$ with $K = K_i$.

We inferred three networks, one for each subtype of subjects using the procedure outlined in §2.2. Note that for different nodes we have different number of attributes, which correspond to medians found by the clustering algorithm. We use the stability selection (Meinshausen and Bühlmann, 2010) approach to estimate stable networks. The stability selection procedure is combined with our estimation procedure as follows. We first select the penalty parameter λ in (4) using cross-validation, which overselects the number of edges in a network. Next, we create 100 subsampled data sets, each of which contain 80% of the data points, and estimate one network for each dataset using the selected λ . The final network is composed of stable edges that appear in at least



(a) Healthy subjects (b) Mild Cognitive Impairment (c) Alzheimer’s & Dementia

Figure 8: Brain connectivity networks

Table 2: Summary statistics for protein, gene, and gene/protein networks ($p = 91$)

	Healthy subjects	Mild Cognitive Impairment	Alzheimer’s & Dementia
Number of edges	116	84	59
Density	0.030	0.020	0.014
Largest connected component	48	27	25
Avg Node Degree	2.40	1.73	1.2
Avg Clustering Coefficient	0.001	0.0023	0.0007

95 of the estimated networks.

We visualize the estimated networks in Figure 8. Table 2 provides a few summary statistics for the estimated networks. Appendix D contains names of different regions, as well as the adjacency matrices for networks. From the summary statistics, we can observe that in normal subjects there are many more connections between different regions of the brain. Loss of connectivity in Alzheimer’s & Dementia has been widely reported in the literature (Greicius et al., 2004, Hedden et al., 2009, Andrews-Hanna et al., 2007, Wu et al., 2011).

Learning functional brain connectivity is potentially valuable for early identification of signs of Alzheimer’s disease. Huang et al. (2009) approach this problem using exploratory data analysis. The framework of Gaussian graphical models is used to explore functional brain connectivity. Here we point out that our approach can be used for the same exploratory task, without the need to reduce the information in the whole brain to one number. For example, from our estimates, we observe the loss of connectivity in the cerebellum region of patients with Alzheimer’s disease, which has been reported previously in Sjöbeck and Englund (2001). As another example, we note increased connectivity between the frontal lobe and other regions in the patients, which was linked to compensation for the lost connections in other regions (Stern, 2006, Gould et al., 2006).

Acknowledgments

We thank Eric D. Kolaczyk and Natallia V. Katenka for sharing preprocessed data used in their study with us. Eric P. Xing is partially supported through the grants NIH R01GM087694 and AFOSR FA9550010247. The research of Han Liu is supported by NSF grant IIS-1116730.

References

J. R. Andrews-Hanna, A. Z. Snyder, J. L. Vincent, C. Lustig, D. Head, M. E. Raichle, and R.L. Buckner. Disruption of large-scale brain systems in advanced aging. *Neuron*, 56:924–935, 2007.

O. Banerjee, L. El Ghaoui, and A. dAspremont. Model selection through sparse maximum likelihood estimation. *J. Mach. Learn. Res.*, 9:485–516, 2008.

- A. Beck and M. Teboulle. A fast iterative shrinkage-thresholding algorithm for linear inverse problems. *SIAM J. Imag. Sci.*, 2:183–202, 2009.
- T. Cai, W. Liu, and X. Luo. A constrained ℓ_1 minimization approach to sparse precision matrix estimation. *J. Am. Statist. Assoc.*, 106:594–607, 2011.
- J. Chiquet, Y. Grandvalet, and C. Ambroise. Inferring multiple graphical structures. *Stat. Comput.*, 21(4):537–553, 2011.
- P. Danaher, P. Wang, and D. M. Witten. The joint graphical lasso for inverse covariance estimation across multiple classes. Technical report, University of Washington, 2011.
- Arthur P. Dempster. Covariance selection. *Biometrics*, 28:157–175, 1972.
- J. H. Friedman, T. J. Hastie, and R. J. Tibshirani. Sparse inverse covariance estimation with the graphical lasso. *Biostatistics*, 9(3):432–441, 2008.
- R. L. Gould, B. Arroyo, R. G. Brown, A. M. Owen, E. T. Bullmore, and R. J. Howard. Brain mechanisms of successful compensation during learning in alzheimer disease. *Neurology*, 67(6):1011–1017, 2006.
- M. D. Greicius, G. Srivastava, A. L. Reiss, and V. Menon. Default-mode network activity distinguishes alzheimer’s disease from healthy aging: evidence from functional mri. *Proc. Natl. Acad. Sci. USA*, 101(13):4637–4642, 2004.
- J. Guo, E. Levina, G. Michailidis, and J. Zhu. Joint estimation of multiple graphical models. *Biometrika*, 98(1):1–15, 2011.
- T. Hedden, K. R. A. Van Dijk, J. A. Becker, A. Mehta, R. A. Sperling, K. A. Johnson, and R. L. Buckner. Disruption of functional connectivity in clinically normal older adults harboring amyloid burden. *J. Neurosci.*, 29(40):12686–12694, 2009.
- Jean Honorio and Dimitris Samaras. Multi-task learning of Gaussian graphical models. In Johannes Fürnkranz and Thorsten Joachims, editors, *Proc. 27 Int. Conf. Mach. Learn.*, pages 447–454. Omnipress, Haifa, Israel, June 2010.
- Shuai Huang, Jing Li, Liang Sun, Jun Liu, Teresa Wu, Kewei Chen, Adam Fleisher, Eric Reiman, and Jieping Ye. Learning brain connectivity of alzheimer’s disease from neuroimaging data. In Y. Bengio, D. Schuurmans, J. Lafferty, C. K. I. Williams, and A. Culotta, editors, *Adv. Neural Inf. Proc. Sys. 22*, pages 808–816. 2009.
- C. Johnson, A. Jalali, and P. Ravikumar. High-dimensional sparse inverse covariance estimation using greedy methods. In Neil Lawrence and Mark Girolami, editors, *Proc. 15 Int. Conf. Artif. Intel. Statist.*, pages 574–582. 2012.
- Natallia Katenka and Eric D. Kolaczyk. Multi-attribute networks and the impact of partial information on inference and characterization. *Ann. Appl. Stat.*, 6(3):1068–1094, 2011.

- Mladen Kolar and Eric P. Xing. Consistent covariance selection from data with missing values. In John Langford and Joelle Pineau, editors, *Proc. 29 Int. Conf. Mach. Learn.*, pages 551–558, New York, NY, USA, July 2012. Omnipress. ISBN 978-1-4503-1285-1.
- Mladen Kolar, Le Song, Amr Ahmed, and Eric P. Xing. Estimating Time-Varying networks. *Ann. Appl. Statist.*, 4(1):94–123, 2010.
- Clifford Lam and Jianqing Fan. Sparsistency and rates of convergence in large covariance matrix estimation. *Ann. Statist.*, 37:4254–4278, 2009.
- S. L. Lauritzen. *Graphical Models (Oxford Statistical Science Series)*. Oxford University Press, USA, July 1996.
- H. Li and J. Gui. Gradient directed regularization for sparse Gaussian concentration graphs, with applications to inference of genetic networks. *Biostatistics*, 7(2):302–317, 2006.
- Karim Lounici, Massimiliano Pontil, Alexandre B Tsybakov, and Sara van de Geer. Oracle inequalities and optimal inference under group sparsity. *Ann. Statist.*, 39: 2164–204, 2011.
- R. Mazumder and D. K. Agarwal. A flexible, scalable and efficient algorithmic framework for primal graphical lasso. Technical report, Stanford University, 2011.
- R. Mazumder and T. J. Hastie. Exact covariance thresholding into connected components for large-scale graphical lasso. *J. Mach. Learn. Res.*, 13:781–794, 2012.
- N. Meinshausen and P. Bühlmann. High dimensional graphs and variable selection with the lasso. *Ann. Statist.*, 34(3):1436–1462, 2006.
- N. Meinshausen and P. Bühlmann. Stability selection. *J. R. Statist. Soc. B*, 72(4): 417–473, 2010.
- Jie Peng, Pei Wang, Nengfeng Zhou, and Ji Zhu. Partial correlation estimation by joint sparse regression models. *J. Am. Statist. Assoc.*, 104(486):735–746, 2009.
- B. Rao. Partial canonical correlations. *Trabajos de Estadística y de Investigación Operativa*, 20(2):211–219, 1969.
- P. Ravikumar, M. J. Wainwright, G. Raskutti, and B. Yu. High-dimensional covariance estimation by minimizing ℓ_1 -penalized log-determinant divergence. *Electron. J. Statist.*, 5:935–980, 2011.
- X. Shen, W. Pan, and Y. Zhu. Likelihood-based selection and sharp parameter estimation. *J. Am. Statist. Assoc.*, 107:223–232, 2012.

- Martin Sjöbeck and Elisabet Englund. Alzheimer’s disease and the cerebellum: a morphologic study on neuronal and glial changes. *Dementia and geriatric cognitive disorders*, 12(3):211–218, 2001.
- Yaakov Stern. Cognitive reserve and alzheimer disease. *Alzheimer Disease & Associated Disorders*, 20(2):112–117, 2006.
- P. Tseng. Convergence of a block coordinate descent method for nondifferentiable minimization. *J. Optim. Theory Appl.*, 109(3):475–494, 2001.
- Gael Varoquaux, Alexandre Gramfort, Jean-Baptiste Poline, and Bertrand Thirion. Brain covariance selection: better individual functional connectivity models using population prior. In J. Lafferty, C. K. I. Williams, J. Shawe-Taylor, R.S. Zemel, and A. Culotta, editors, *Adv. Neural Inf. Proc. Sys. 23*, pages 2334–2342. 2010.
- D. M. Witten, J. H. Friedman, and N. Simon. New insights and faster computations for the graphical lasso. *J. Comput. Graph. Stat.*, 20(4):892–900, 2011.
- X. Wu, R. Li, A. S. Fleisher, E. M. Reiman, X. Guan, Y. Zhang, K. Chen, and L. Yao. Altered default mode network connectivity in alzheimer’s diseasea resting functional mri and bayesian network study. *Human brain mapping*, 32(11):1868–1881, 2011.
- Ming Yuan. High dimensional inverse covariance matrix estimation via linear programming. *J. Mach. Learn. Res.*, 11:2261–2286, 2010.
- Ming Yuan and Yi Lin. Model selection and estimation in regression with grouped variables. *J. R. Statist. Soc. B*, 68:49–67, 2006.
- Ming Yuan and Yi Lin. Model selection and estimation in the gaussian graphical model. *Biometrika*, 94(1):19–35, 2007.
- T. Zhao, H. Liu, K. E. Roeder, J. D. Lafferty, and L. A. Wasserman. The huge package for high-dimensional undirected graph estimation in r. *J. Mach. Learn. Res.*, 13: 1059–1062, 2012.

A Efficient Updates of the Precision and Covariance Matrices

Our algorithm consists of updating the precision matrix by solving optimization problems (7) and (8) and then updating the estimate of the covariance matrix. Both steps can be performed efficiently.

Solutions to (7) and (8) can be computed in a closed form as

$$\hat{\Omega}_{aa} = (1 - t\lambda/|\tilde{\Omega}_{aa} + t(\tilde{\Sigma}_{aa} - S_{aa})|_F)_+(\tilde{\Omega}_{aa} + t(\tilde{\Sigma}_{aa} - S_{aa})), \quad \text{and} \quad (11)$$

$$\hat{\Omega}_{ab} = (1 - t\lambda/|\tilde{\Omega}_{ab} + t(\tilde{\Sigma}_{ab} - S_{ab})|_F)_+(\tilde{\Omega}_{ab} + t(\tilde{\Sigma}_{ab} - S_{ab})), \quad \forall b \in \bar{a}, \quad (12)$$

where $(x)_+ = \max(0, x)$.

The estimate of the covariance matrix can be updated efficiently, without inverting the whole $\hat{\Omega}$ matrix, using the matrix inversion lemma as follows

$$\begin{aligned} \hat{\Sigma}_{\bar{a},\bar{a}} &= (\tilde{\Omega}_{\bar{a},\bar{a}})^{-1} + (\tilde{\Omega}_{\bar{a},\bar{a}})^{-1}\hat{\Omega}_{\bar{a},a}(\hat{\Omega}_{aa} - \hat{\Omega}_{a,\bar{a}}(\tilde{\Omega}_{\bar{a},\bar{a}})^{-1}\hat{\Omega}_{\bar{a},a})^{-1}\hat{\Omega}_{a,\bar{a}}(\tilde{\Omega}_{\bar{a},\bar{a}})^{-1}, \\ \hat{\Sigma}_{a,\bar{a}} &= -\hat{\Omega}_{aa}\hat{\Omega}_{a,\bar{a}}\hat{\Sigma}_{\bar{a},\bar{a}}, \\ \hat{\Sigma}_{aa} &= (\hat{\Omega}_{aa} - \hat{\Omega}_{a,\bar{a}}(\tilde{\Omega}_{\bar{a},\bar{a}})^{-1}\hat{\Omega}_{\bar{a},a})^{-1}, \end{aligned} \quad (13)$$

with $(\tilde{\Omega}_{\bar{a},\bar{a}})^{-1} = \tilde{\Sigma}_{\bar{a},\bar{a}} - \tilde{\Sigma}_{\bar{a},a}\tilde{\Sigma}_{aa}^{-1}\tilde{\Sigma}_{a,\bar{a}}$.

B Complexity Analysis of Multi-attribute Estimation

Step 2 of the estimation algorithm updates portions of the precision and covariance matrices corresponding to one node at a time. From §A, we observe that the computational complexity of updating the precision matrix is $\mathcal{O}(pk^2)$. Updating the covariance matrix requires computing $(\tilde{\Omega}_{\bar{a},\bar{a}})^{-1}$, which can be efficiently done in $\mathcal{O}(p^2k^2 + pk^2 + k^3) = \mathcal{O}(p^2k^2)$ operations, assuming that $k \ll p$. With this, the covariance matrix can be updated in $\mathcal{O}(p^2k^2)$ operations. Therefore the total cost of updating the covariance and precision matrices is $\mathcal{O}(p^2k^2)$ operations. Since step 2 needs to be performed for each node $a \in V$, the total complexity is $\mathcal{O}(p^3k^2)$. Let T denote the total number of times step 2 is executed. This leads to the overall complexity of the algorithm as $\mathcal{O}(Tp^3k^2)$. In practice, we observe that $T \approx 10$ to 20 for sparse graphs. Furthermore, when the whole solution path is computed, we can use warm starts to further speed up computation, leading to $T < 5$ for each λ .

C Technical Proofs

In this appendix, we collect proofs of the results presented in the main part of the paper.

C.1 Proof of Lemma 1

We start the proof by giving to technical results needed later. The following lemma states that the minimizer of (4) is unique and has bounded minimum and maximum eigenvalues, denoted as Λ_{\min} and Λ_{\max} .

Lemma 5. *For every value of $\lambda > 0$, the optimization problem in Eq. (4) has a unique minimizer $\hat{\Omega}$, which satisfies $\Lambda_{\min}(\hat{\Omega}) \geq (\Lambda_{\max}(S) + \lambda p)^{-1} > 0$ and $\Lambda_{\max}(\hat{\Omega}) \leq \lambda^{-1} \sum_{j \in V} k_j$.*

Proof. The optimization objective given in (4) can be written in the equivalent constrained form as

$$\min_{\Omega > 0} \text{tr } S\Omega - \log |\Omega| \quad \text{subject to} \quad \sum_{a,b} \|\Omega_{ab}\|_F \leq C(\lambda).$$

The procedure involves minimizing a continuous objective over a compact set, and so by Weierstrass theorem, the minimum is always achieved. Furthermore, the objective is strongly convex and therefore the minimum is unique.

The solution $\hat{\Omega}$ to the optimization problem (4) satisfies

$$S - \hat{\Omega}^{-1} + \lambda Z = 0 \tag{14}$$

where $Z \in \partial \sum_{a,b} \|\hat{\Omega}_{ab}\|_F$ is the element of the sub-differential and satisfies $\|Z_{ab}\|_F \leq 1$ for all $(a, b) \in V^2$. Therefore,

$$\Lambda_{\max}(\hat{\Omega}^{-1}) \leq \Lambda_{\max}(S) + \lambda \Lambda_{\max}(Z) \leq \Lambda_{\max}(S) + \lambda p.$$

Next, we prove an upper bound on $\Lambda_{\max}(\hat{\Omega})$. At optimum, the primal-dual gap is zero, which gives that

$$\sum_{a,b} \|\hat{\Omega}_{ab}\|_F \leq \lambda^{-1} \left(\sum_{j \in V} k_j - \text{tr } S\hat{\Omega} \right) \leq \lambda^{-1} \sum_{j \in V} k_j,$$

as $S \geq 0$ and $\hat{\Omega} > 0$. Since $\Lambda_{\max}(\hat{\Omega}) \leq \sum_{a,b} \|\hat{\Omega}_{ab}\|_F$, the proof is done. \square

The next results states that the objective function has a Lipschitz continuous gradient, which will be used to show that the generalized gradient descent can be used to find $\hat{\Omega}$.

Lemma 6. *The function $f(A) = \text{tr } SA - \log |A|$ has a Lipschitz continuous gradient on the set $\{A \in \mathcal{S}^p : \Lambda_{\min}(A) \geq \gamma\}$, with the Lipschitz constant $L = \gamma^{-2}$.*

Proof. We have that $\nabla f(A) = S - A^{-1}$. Then

$$\begin{aligned} \|\nabla f(A) - \nabla f(A')\|_F &= \|A^{-1} - (A')^{-1}\|_F \\ &\leq \Lambda_{\max} A^{-1} \|A - A'\|_F \Lambda_{\max} A^{-1} \\ &\leq \gamma^{-2} \|A - A'\|_F, \end{aligned}$$

which completes the proof. \square

Now, we provide the proof of Lemma 1.

By construction, the sequence of estimates $(\tilde{\Omega}^{(t)})_{t \geq 1}$ decrease the objective value and are positive definite.

To prove the convergence, we first introduce some additional notation. Let $f(\Omega) = \text{tr } S\Omega - \log |\Omega|$ and $F(\Omega) = f(\Omega) + \sum_{ab} \|\Omega_{ab}\|_F$. For any $L > 0$, let

$$Q_L(\Omega; \bar{\Omega}) := f(\bar{\Omega}) + \text{tr}[(\Omega - \bar{\Omega})\nabla f(\bar{\Omega})] + \frac{L}{2}\|\Omega - \bar{\Omega}\|_F^2 + \sum_{ab} \|\Omega_{ab}\|_F$$

be a quadratic approximation of $F(\Omega)$ at a given point $\bar{\Omega}$, which has a unique minimizer

$$p_L(\bar{\Omega}) := \arg \min_{\Omega} Q_L(\Omega; \bar{\Omega}).$$

From Lemma 2.3. in Beck and Teboulle (2009), we have that

$$F(\bar{\Omega}) - F(p_L(\bar{\Omega})) \geq \frac{L}{2}\|p_L(\bar{\Omega}) - \bar{\Omega}\|_F^2 \quad (15)$$

if $F(p_L(\bar{\Omega})) \leq Q_L(p_L(\bar{\Omega}); \bar{\Omega})$. Note that $F(p_L(\bar{\Omega})) \leq Q_L(p_L(\bar{\Omega}); \bar{\Omega})$ always holds if L is as large as the Lipschitz constant of ∇F .

Let $\tilde{\Omega}^{(t-1)}$ and $\tilde{\Omega}^{(t)}$ denote two successive iterates obtained by the procedure. Without loss of generality, we can assume that $\tilde{\Omega}^{(t)}$ is obtained by updating the rows/columns corresponding to the node a . From (15), it follows that

$$\frac{2}{L_k}(F(\tilde{\Omega}^{(t-1)}) - F(\tilde{\Omega}^{(t)})) \geq \|\tilde{\Omega}_{aa}^{(t-1)} - \tilde{\Omega}_{aa}^{(t)}\|_F + 2 \sum_{b \neq a} \|\tilde{\Omega}_{ab}^{(t-1)} - \tilde{\Omega}_{ab}^{(t)}\|_F \quad (16)$$

where L_k is a current estimate of the Lipschitz constant. Recall that in our procedure the scalar t serves as a local approximation of $1/L$. Since eigenvalues of $\hat{\Omega}$ are bounded according to Lemma 5, we can conclude that the eigenvalues of $\tilde{\Omega}^{(t-1)}$ are bounded as well. Therefore the current Lipschitz constant is bounded away from zero, using Lemma 6. Combining the results, we observe that the right hand side of (16) converges to zero as $t \rightarrow \infty$, since the optimization procedure produces iterates that decrease the objective value. This shows that $\|\tilde{\Omega}_{aa}^{(t-1)} - \tilde{\Omega}_{aa}^{(t)}\|_F + 2 \sum_{b \neq a} \|\tilde{\Omega}_{ab}^{(t-1)} - \tilde{\Omega}_{ab}^{(t)}\|_F$ converges to zero, for any $a \in V$. Since $(\tilde{\Omega}^{(t)})$ is a bounded sequence, it has a limit point, which we denote $\hat{\Omega}$. It is easy to see, from the stationary conditions for the optimization problem given in (6), that the limit point $\hat{\Omega}$ also satisfies the global KKT conditions to the optimization problem in (4).

C.2 Proof of Lemma 3

Suppose that the solution $\hat{\Omega}$ to (4) is block diagonal with blocks P_1, P_2, \dots, P_l . For two nodes a, b in different blocks, we have that $(\hat{\Omega})_{ab}^{-1} = 0$ as the inverse of the block diagonal matrix is block diagonal. From the KKT conditions, it follows that $\|S_{ab}\|_F \leq \lambda$.

Now suppose that $\|S_{ab}\|_F \leq \lambda$ for all $a \in P_j, b \in P_{j'}, j \neq j'$. For every $l' = 1, \dots, l$ construct

$$\tilde{\Omega}_{l'} = \arg \min_{\Omega_{l'} > 0} \text{tr} S_{l'} \Omega_{l'} - \log |\Omega_{l'}| + \lambda \sum_{a,b} \|\Omega_{ab}\|_F.$$

Then $\hat{\Omega} = \text{diag}(\hat{\Omega}_1, \hat{\Omega}_2, \dots, \hat{\Omega}_l)$ is the solution of (4) as it satisfies the KKT conditions.

C.3 Proof of Eq. (3)

First, we note that

$$\text{var}((X_a^T, X_b^T)^T | X_{\overline{ab}}) = \Sigma_{ab,ab} - \Sigma_{ab,\overline{ab}} \Sigma_{\overline{ab},\overline{ab}}^{-1} \Sigma_{\overline{ab},ab}$$

is the conditional covariance matrix of $(X_a^T, X_b^T)^T$ given the remaining nodes $X_{\overline{ab}}$ (see Proposition C.5 in Lauritzen (1996)). Define $\overline{\Sigma} = \Sigma_{ab,ab} - \Sigma_{ab,\overline{ab}} \Sigma_{\overline{ab},\overline{ab}}^{-1} \Sigma_{\overline{ab},ab}$. Partial canonical correlation between X_a and X_b is equal to zero if and only if $\overline{\Sigma}_{ab} = 0$. On the other hand, the matrix inversion lemma gives that $\Omega_{ab,ab} = \overline{\Sigma}^{-1}$. Now, $\Omega_{ab} = 0$ if and only if $\overline{\Sigma}_{ab} = 0$. This shows the equivalence relationship in Eq. (3).

C.4 Proof of Proposition 4

We provide sufficient conditions for consistent network estimation. Proposition 4 given in §3 is then a simple consequence. To provide sufficient conditions, we extend the work of Ravikumar et al. (2011) to our setting, where we observe multiple attributes for each node. In particular, we extend their Theorem 1.

For simplicity of presentation, we assume that $k_a = k$, for all $a \in V$, that is, we assume that the same number of attributes is observed for each node. Our assumptions involve the Hessian of the function $f(A) = \text{tr} SA - \log |A|$ evaluated at the true Ω^* ,

$$\mathcal{H} = \mathcal{H}(\Omega^*) = (\Omega^*)^{-1} \otimes (\Omega^*)^{-1} \in \mathbb{R}^{(pk)^2 \times (pk)^2}, \quad (17)$$

and the true covariance matrix Σ^* . The Hessian and the covariance matrix can be thought of block matrices with blocks of size $k^2 \times k^2$ and $k \times k$, respectively. We will make use of the operator $\mathcal{C}(\cdot)$ that operates on these block matrices and outputs a smaller matrix with elements that equal to the Frobenius norm of the original blocks,

$$\begin{pmatrix} A_{11} & A_{12} & \cdots & A_{1p} \\ A_{21} & A_{22} & \cdots & A_{2p} \\ \vdots & & \ddots & \vdots \\ A_{p1} & \cdots & & A_{pp} \end{pmatrix} \xrightarrow{\mathcal{C}(\cdot)} \begin{pmatrix} \|A_{11}\|_F & \|A_{12}\|_F & \cdots & \|A_{1p}\|_F \\ \|A_{21}\|_F & \|A_{22}\|_F & \cdots & \|A_{2p}\|_F \\ \vdots & & \ddots & \vdots \\ \|A_{p1}\|_F & \cdots & & \|A_{pp}\|_F \end{pmatrix}$$

In particular, $\mathcal{C}(\Sigma^*) \in \mathbb{R}^{p \times p}$ and $\mathcal{C}(\mathcal{H}) \in \mathbb{R}^{p^2 \times p^2}$.

We denote the index set of the non-zero blocks of the precision matrix as

$$\mathcal{T} := \{(a, b) \in V \times V : \|\Omega_{ab}^*\|_2 \neq 0\} \cup \{(a, a) : a \in V\}$$

and let \mathcal{N} denote its complement in $V \times V$, that is,

$$\mathcal{N} = \{(a, b) : \|\Omega_{ab}\|_F = 0\}.$$

As mentioned earlier, we need to make an assumption on the Hessian matrix, which takes the standard irrepresentable-like form. There exists a constant $\alpha \in [0, 1)$ such that

$$\|\mathcal{C}(\mathcal{H}_{\mathcal{N}\mathcal{T}}(\mathcal{H}_{\mathcal{T}\mathcal{T}})^{-1})\|_\infty \leq 1 - \alpha. \quad (18)$$

These condition extends the irrepresentable condition given in Ravikumar et al. (2011), which was needed for estimation of networks from single attribute observations. It is worth noting, that the condition given in Eq. (18) can be much weaker than the irrepresentable condition of Ravikumar et al. (2011) applied directly to the full Hessian matrix. This can be observed in simulations done in §5, where a chain network is not consistently estimated even with a large number of samples.

We will also need the following two quantities to specify the results

$$\kappa_{\Sigma^*} = \|\mathcal{C}(\Sigma^*)\|_\infty \quad (19)$$

and

$$\kappa_{\mathcal{H}} = \|\mathcal{C}(\mathcal{H}_{\mathcal{T}\mathcal{T}}^{-1})\|_\infty. \quad (20)$$

Finally, the results are going to depend on the tail bounds for the elements of the matrix $\mathcal{C}(S - \Sigma^*)$. We will assume that there is a constant $v_* \in (0, \infty]$ and a function $f : \mathbb{N} \times (0, \infty) \mapsto (0, \infty)$ such that for any $(a, b) \in V \times V$

$$\text{pr}(\mathcal{C}(S - \Sigma^*)_{ab} \geq \delta) \leq \frac{1}{f(n, \delta)} \quad \delta \in (0, v_*^{-1}]. \quad (21)$$

The function $f(n, \delta)$ will be monotonically increasing in both n and δ . Therefore, we define the following two inverse functions

$$\bar{n}_f(\delta; r) = \arg \max\{n : f(n, \delta) \leq r\} \quad (22)$$

and

$$\bar{\delta}_f(r; n) = \arg \max\{\delta : f(n, \delta) \leq r\} \quad (23)$$

for $r \in [1, \infty)$.

With the notation introduced, we have the following result.

Theorem 7. *Assume that the irrepresentable condition in Eq. (18) is satisfied and that there exists a constant $v_* \in (0, \infty]$ and a function $f(n, \delta)$ so that Eq. (21) is satisfied for any $(a, b) \in V \times V$. Let*

$$\lambda = \frac{8}{\alpha} \bar{\delta}_f(n, p^\tau)$$

for some $\tau > 2$. If

$$n > \bar{n}_f\left(\frac{1}{\max(v_*, 6(1 + 8\alpha^{-1})s \max(\kappa_{\Sigma^*} \kappa_{\mathcal{H}}, \kappa_{\Sigma^*}^3 \kappa_{\mathcal{H}}^2))}, p^\tau\right) \quad (24)$$

then

$$\|\mathcal{C}(\widehat{\Omega} - \Omega)\|_\infty \leq 2(1 + 8\alpha^{-1})\kappa_{\mathcal{H}}\bar{\delta}_f(n, p^\tau) \quad (25)$$

with probability at least $1 - p^{2-\tau}$.

Theorem 7 is of the same form as Theorem 1 in Ravikumar et al. (2011), but the ℓ_∞ element-wise convergence is established for $\mathcal{C}(\widehat{\Omega} - \Omega)$, which will guarantee successful recovery of non-zero partial canonical correlations if the blocks of the true precision matrix are sufficiently large.

Theorem 7 is proven as Theorem 1 in Ravikumar et al. (2011). We provide technical results in Lemma 8, Lemma 9 and Lemma 10, which can be used to substitute results of Lemma 4, Lemma 5 and Lemma 6 in Ravikumar et al. (2011) under our setting. The rest of the arguments then go through. Below we provide some more details.

First, let $\mathcal{Z} : \mathbb{R}^{pk \times pk} \mapsto \mathbb{R}^{pk \times pk}$ be the mapping defined as

$$\mathcal{Z}(A)_{ab} = \begin{cases} \frac{A_{ab}}{\|A_{ab}\|_F} & \text{if } \|A_{ab}\|_F \neq 0, \\ Z \text{ with } \|Z\|_F \leq 1 & \text{if } \|A_{ab}\|_F = 0, \end{cases} \quad (26)$$

Next, define the function

$$G(\Omega) = \text{tr } \Omega S - \log |\Omega| + \lambda \|\mathcal{C}(\Omega)\|_1, \quad \forall \Omega > 0 \quad (27)$$

and the following system of equations

$$\begin{cases} S_{ab} - (\Omega^{-1})_{ab} = -\lambda \mathcal{Z}(\Omega)_{ab}, & \text{if } \Omega_{ab} \neq 0 \\ \|\mathcal{Z}(\Omega)_{ab}\|_F \leq \lambda, & \text{if } \Omega_{ab} = 0. \end{cases} \quad (28)$$

It is known that $\Omega \in \mathbb{R}^{\tilde{p} \times \tilde{p}}$ is the minimizer of optimization problem in Eq. (4) if and only if it satisfies the system of equations given in Eq. (28). We have already shown in Lemma 5 that the minimizer is unique.

Let $\tilde{\Omega}$ be the solution to the following constrained optimization problem

$$\min_{\Omega > 0} \text{tr } S\Omega - \log |\Omega| + \lambda \|\mathcal{C}(\Omega)\|_1 \text{ subject to } \mathcal{C}(\Omega)_{ab} = 0, \forall (a, b) \in \mathcal{N}. \quad (29)$$

Observe that one cannot find $\tilde{\Omega}$ in practice, as it depends on the unknown set \mathcal{N} . However, it is a useful construction in the proof. We will prove that $\tilde{\Omega}$ is solution to the optimization problem given in Eq. (4), that is, we will show that $\tilde{\Omega}$ satisfies the system of equations (28).

Using the first-order Taylor expansion we have that

$$\tilde{\Omega}^{-1} = (\Omega^*)^{-1} - (\Omega^*)^{-1} \Delta (\Omega^*)^{-1} + R(\Delta), \quad (30)$$

where $\Delta = \Omega - \Omega^*$ and $R(\Delta)$ denotes the remainder term. With this, we state and prove Lemma 8, Lemma 9 and Lemma 10. They can be combined as in Ravikumar et al. (2011) to complete the proof of Theorem 7.

Lemma 8. *Assume that*

$$\max_{ab} \|\Delta_{ab}\|_F \leq \frac{\alpha\lambda}{8} \quad \text{and} \quad \max_{ab} \|\Sigma_{ab}^* - S_{ab}\|_F \leq \frac{\alpha\lambda}{8}. \quad (31)$$

Then $\tilde{\Omega}$ is the solution to the optimization problem in Eq. (4).

Proof. We use R to denote $R(\Delta)$. Recall that $\Delta_{\mathcal{N}} = 0$ by construction. Using (30) we can rewrite (28) as

$$\mathcal{H}_{ab,\mathcal{T}} \bar{\Delta}_{\mathcal{T}} - \bar{R}_{ab} + \bar{S}_{ab} - \bar{\Sigma}_{ab}^* + \lambda \bar{\mathcal{Z}}(\tilde{\Omega})_{ab} = 0 \quad \text{if } (a, b) \in \mathcal{T} \quad (32)$$

$$\|\mathcal{H}_{ab,\mathcal{T}} \bar{\Delta}_{\mathcal{T}} - \bar{R}_{ab} + \bar{S}_{ab} - \bar{\Sigma}_{ab}^*\|_2 \leq \lambda \quad \text{if } (a, b) \in \mathcal{N}. \quad (33)$$

By construction, the solution $\tilde{\Omega}$ satisfy (32). Under the assumptions, we show that (33) is also satisfied with inequality.

From (32), we can solve for $\Delta_{\mathcal{T}}$,

$$\Delta_{\mathcal{T}} = \mathcal{H}_{\mathcal{T},\mathcal{T}}^{-1} [\bar{R}_{\mathcal{T}} - \bar{\Sigma}_{\mathcal{T}} + \bar{S}_{\mathcal{T}} - \lambda \bar{\mathcal{Z}}(\tilde{\Omega})_{\mathcal{T}}].$$

Then

$$\begin{aligned} & \|\mathcal{H}_{ab,\mathcal{T}} \mathcal{H}_{\mathcal{T},\mathcal{T}}^{-1} [\bar{R}_{\mathcal{T}} - \bar{\Sigma}_{\mathcal{T}} + \bar{S}_{\mathcal{T}} - \lambda \bar{\mathcal{Z}}(\tilde{\Omega})_{\mathcal{T}}] - \bar{R}_{ab} + \bar{S}_{ab} - \bar{\Sigma}_{ab}^*\|_2 \\ & \leq \lambda \|\mathcal{H}_{ab,\mathcal{T}} \mathcal{H}_{\mathcal{T},\mathcal{T}}^{-1} \bar{\mathcal{Z}}(\tilde{\Omega})_{\mathcal{T}}\|_2 + \|\mathcal{H}_{ab,\mathcal{T}} \mathcal{H}_{\mathcal{T},\mathcal{T}}^{-1} [\bar{R}_{\mathcal{T}} - \bar{\Sigma}_{\mathcal{T}} + \bar{S}_{\mathcal{T}}]\|_2 + \|\bar{R}_{ab} + \bar{S}_{ab} - \bar{\Sigma}_{ab}^*\|_2 \\ & \leq \lambda(1 - \alpha) + (2 - \alpha) \frac{\alpha\lambda}{4} \\ & < \lambda \end{aligned}$$

using assumption on \mathcal{H} in (18) and (31). This shows that $\tilde{\Omega}$ satisfies (28). \square

Lemma 9. *Assume that*

$$\|\mathcal{C}(\Delta)\|_{\infty} \leq \frac{1}{3\kappa_{\Sigma^*} s}. \quad (34)$$

Then

$$\|\mathcal{C}(R(\Delta))\|_{\infty} \leq \frac{3s}{2} \kappa_{\Sigma^*}^3 \|\mathcal{C}(\Delta)\|_{\infty}^2. \quad (35)$$

Proof. Remainder term can be written as

$$R(\Delta) = (\Omega^* + \Delta)^{-1} - (\Omega^*)^{-1} + (\Omega^*)^{-1} \Delta (\Omega^*)^{-1}.$$

Using (40), we have that

$$\begin{aligned} \|\mathcal{C}((\Omega^*)^{-1} \Delta)\|_{\infty} & \leq \|\mathcal{C}((\Omega^*)^{-1})\|_{\infty} \|\mathcal{C}(\Delta)\|_{\infty} \\ & \leq s \|\mathcal{C}((\Omega^*)^{-1})\|_{\infty} \|\mathcal{C}(\Delta)\|_{\infty} \\ & \leq \frac{1}{3} \end{aligned}$$

which gives us the following expansion

$$(\Omega^* + \Delta)^{-1} = (\Omega^*)^{-1} - (\Omega^*)^{-1}\Delta(\Omega^*)^{-1} + (\Omega^*)^{-1}\Delta(\Omega^*)^{-1}\Delta J(\Omega^*)^{-1},$$

with $J = \sum_{k \geq 0} (-1)^k ((\Omega^*)^{-1}\Delta)^k$. Using (41) and (40), we have that

$$\begin{aligned} \|\mathcal{C}(R)\|_\infty &\leq \|\mathcal{C}((\Omega^*)^{-1}\Delta)\|_\infty \|\mathcal{C}((\Omega^*)^{-1}\Delta J(\Omega^*)^{-1})^T\|_\infty \\ &\leq \|\mathcal{C}((\Omega^*)^{-1})\|_\infty^3 \|\mathcal{C}(\Delta)\|_\infty \|\mathcal{C}(J^T)\|_\infty \|\mathcal{C}(\Delta)\|_\infty \\ &\leq s \|\mathcal{C}((\Omega^*)^{-1})\|_\infty^3 \|\mathcal{C}(\Delta)\|_\infty^2 \|\mathcal{C}(J^T)\|_\infty. \end{aligned}$$

Next, we have that

$$\begin{aligned} \|\mathcal{C}(J^T)\|_\infty &\leq \sum_{k > 0} \|\mathcal{C}(\Delta(\Omega^*)^{-1})\|_\infty^k \\ &\leq \frac{1}{1 - \|\mathcal{C}(\Delta(\Omega^*)^{-1})\|_\infty} \\ &\leq \frac{3}{2}, \end{aligned}$$

which gives us

$$\|\mathcal{C}(R)\|_\infty \leq \frac{3s}{2} \kappa_{\Sigma^*}^3 \|\mathcal{C}(\Delta)\|_\infty^2$$

as claimed. \square

Lemma 10. *Assume that*

$$r := 2\kappa_{\mathcal{H}}(\|\mathcal{C}(S - \Sigma^*)\|_\infty + \lambda) \leq \min\left(\frac{1}{3\kappa_{\Sigma^*} s}, \frac{1}{3\kappa_{\mathcal{H}} \kappa_{\Sigma^*}^3 s}\right). \quad (36)$$

Then

$$\|\mathcal{C}(\Delta)\|_\infty \leq r. \quad (37)$$

Proof. The proof follows the proof of Lemma 6 in Ravikumar et al. (2011). Define the ball

$$\mathcal{B}(r) := \{A : \mathcal{C}(A)_{ab} \leq r, \forall (a, b) \in \mathcal{T}\},$$

the gradient mapping

$$G(\Omega_{\mathcal{T}}) = -(\Omega^{-1})_{\mathcal{T}} + S_{\mathcal{T}} + \lambda \mathcal{Z}(\Omega)_{\mathcal{T}}$$

and

$$F(\overline{\Delta}_{\mathcal{T}}) = -\mathcal{H}_{\mathcal{T}\mathcal{T}}^{-1} \overline{\mathcal{G}}(\Omega_{\mathcal{T}}^* + \Delta_{\mathcal{T}}) + \overline{\Delta}_{\mathcal{T}}.$$

We need to show that $F(\mathcal{B}(r)) \subseteq \mathcal{B}(r)$, which implies that $\|\mathcal{C}(\Delta_{\mathcal{T}})\|_\infty \leq r$.

Under the assumptions of the lemma, for any $\Delta_S \in \mathcal{B}(r)$, we have the following decomposition

$$F(\overline{\Delta}_{\mathcal{T}}) = \mathcal{H}_{\mathcal{T}\mathcal{T}}^{-1} \overline{\mathcal{R}}(\Delta)_{\mathcal{T}} + \mathcal{H}_{\mathcal{T}\mathcal{T}}^{-1} (\overline{\mathcal{S}}_{\mathcal{T}} - \overline{\Sigma}_{\mathcal{T}}^* + \lambda \overline{\mathcal{Z}}(\Omega^* + \Delta)_{\mathcal{T}}).$$

Using Lemma 9, the first term can be bounded as

$$\begin{aligned}
\|\mathcal{C}(\mathcal{H}_{\mathcal{T}\mathcal{T}}^{-1}\bar{R}(\Delta)_{\mathcal{T}})\|_{\infty} &\leq \|\mathcal{C}(\mathcal{H}_{\mathcal{T}\mathcal{T}}^{-1})\|_{\infty}\|\mathcal{C}(R(\Delta))\|_{\infty} \\
&\leq \frac{3s}{2}\kappa_{\mathcal{H}}\kappa_{\Sigma^*}^3\|\mathcal{C}(\Delta)\|_{\infty}^2 \\
&\leq \frac{3s}{2}\kappa_{\mathcal{H}}\kappa_{\Sigma^*}^3r^2 \\
&\leq r/2
\end{aligned}$$

where the last inequality follows under the assumptions. Similarly

$$\begin{aligned}
&\|\mathcal{C}(\mathcal{H}_{\mathcal{T}\mathcal{T}}^{-1}(\bar{S}_{\mathcal{T}} - \bar{\Sigma}_{\mathcal{T}}^* + \lambda\bar{\mathcal{Z}}(\Omega^* + \Delta)_{\mathcal{T}}))\|_{\infty} \\
&\leq \|\mathcal{C}(\mathcal{H}_{\mathcal{T}\mathcal{T}}^{-1})\|_{\infty}(\|\mathcal{C}(S - \Sigma^*)\|_{\infty} + \lambda\|\mathcal{C}(\mathcal{Z}(\Omega^* + \Delta))\|_{\infty}) \\
&\leq \kappa_{\mathcal{H}}(\|\mathcal{C}(S - \bar{\Sigma}^*)\|_{\infty} + \lambda) \\
&\leq r/2.
\end{aligned}$$

This shows that $F(\mathcal{B}(r)) \subseteq \mathcal{B}(r)$. \square

The following result is a corollary of Theorem 7, which shows that the graph structure can be estimated consistently under some assumptions.

Corollary 11. *Assume that the conditions of Theorem 7 are satisfied. Furthermore, suppose that*

$$\min_{(a,b) \in \mathcal{T}, a \neq b} \|\Omega\|_F > 2(1 + 8\alpha^{-1})\kappa_{\mathcal{H}}\bar{\delta}_f(n, p^{\tau})$$

then Algorithm 1 estimates a graph \hat{G} which satisfies

$$\text{pr}(\hat{G} \neq G) \geq 1 - p^{2-\tau}.$$

Next, we specialize the result of Theorem 7 to a case where X has sub-Gaussian tails. That is, the random vector $X = (X_1, \dots, X_{pk})^T$ is zero-mean with covariance Σ^* . Each $(\sigma_{aa}^*)^{-1/2}X_a$ is sub-Gaussian with parameter γ .

Proposition 12. *Set the penalty parameter in λ in Eq. (4) as*

$$\lambda = 8k\alpha^{-1} \left(128(1 + 4\gamma^2)^2(\max_a \sigma_{aa}^*)^2 n^{-1}(2\log(2k) + \tau\log(p)) \right)^{1/2}.$$

If

$$n > C_1 s^2 k^2 (1 + 8\alpha^{-1})^2 (\tau \log p + \log 4 + 2 \log k)$$

where $C_1 = (48\sqrt{2}(1 + 4\gamma^2)(\max_a \sigma_{aa}^*) \max(\kappa_{\Sigma^*}\kappa_{\mathcal{H}}, \kappa_{\Sigma^*}^3\kappa_{\mathcal{H}}^2))^2$ then

$$\|\mathcal{C}(\hat{\Omega} - \Omega)\|_{\infty} \leq 16\sqrt{2}(1 + 4\gamma^2) \max_i \sigma_{ii}^* (1 + 8\alpha^{-1})\kappa_{\mathcal{H}}k \left(\frac{\tau \log p + \log 4 + 2 \log k}{n} \right)^{1/2}$$

with probability $1 - p^{2-\tau}$.

The proof simply follows by observing that, for any (a, b) ,

$$\begin{aligned}
\text{pr}(\mathcal{C}(S - \Sigma^*)_{ab} > \delta) &\leq \text{pr}\left(\max_{(c,d) \in (a,b)} (\sigma_{cd} - \sigma_{cd}^*)^2 > \delta^2/k^2\right) \\
&\leq k^2 \text{pr}(|\sigma_{cd} - \sigma_{cd}^*| > \delta/k) \\
&\leq 4k^2 \exp\left(-\frac{n\delta^2}{c_*k^2}\right)
\end{aligned} \tag{38}$$

for all $\delta \in (0, 8(1 + 4\gamma^2)(\max_a \sigma_{aa}^*))$ with $c_* = 128(1 + 4\gamma^2)^2(\max_a (\sigma_{aa}^*))^2$. Therefore,

$$\begin{aligned}
f(n, \delta) &= \frac{1}{4k^2} \exp\left(c_* \frac{n\delta^2}{k^2}\right) \\
\bar{n}_f(\delta; r) &= \frac{k^2 \log(4k^2 r)}{c_* \delta^2} \\
\bar{\delta}_f(r; n) &= \left(\frac{k^2 \log(4k^2 r)}{c_* n}\right)^{1/2}.
\end{aligned}$$

Theorem 7 and some simple algebra complete the proof.

Proposition 4 is a simple consequence of Proposition 12.

C.5 Some Results on Norms of Block Matrices

Let \mathcal{T} be a partition of V . Throughout this section, we assume that matrices $A, B \in \mathbb{R}^{p \times p}$ and a vector $b \in \mathbb{R}^p$ are partitioned into blocks according to \mathcal{T} .

Lemma 13.

$$\max_{a \in \mathcal{T}} \|A_a \cdot b\|_2 \leq \max_{a \in \mathcal{T}} \sum_{b \in \mathcal{T}} \|A_{ab}\|_F \max_{c \in \mathcal{T}} \|b_c\|_2. \tag{39}$$

Proof. For any $a \in \mathcal{T}$,

$$\begin{aligned}
\|A_a \cdot b\|_2 &\leq \sum_{b \in \mathcal{T}} \|A_{ab} b_b\|_2 \\
&= \sum_{b \in \mathcal{T}} \left(\sum_{i \in a} (A_{ib} b_b)^2\right)^{1/2} \\
&\leq \sum_{b \in \mathcal{T}} \left(\sum_{i \in a} \|A_{ib}\|_2^2 \|b_b\|_2^2\right)^{1/2} \\
&\leq \sum_{b \in \mathcal{T}} \left(\sum_{i \in a} \|A_{ib}\|_2^2\right)^{1/2} \max_{c \in \mathcal{T}} \|b_c\|_2 \\
&= \sum_{b \in \mathcal{T}} \|A_{ab}\|_F \max_{c \in \mathcal{T}} \|b_c\|_2.
\end{aligned}$$

□

Lemma 14.

$$\|\mathcal{C}(AB)\|_\infty \leq \|\mathcal{C}(B)\|_\infty \|\mathcal{C}(A)\|_\infty. \quad (40)$$

Proof. Let $\mathbf{C} = AB$ and let \mathcal{T} be a partition of V .

$$\begin{aligned} \|\mathcal{C}(AB)\|_\infty &= \max_{a \in \mathcal{T}} \sum_{b \in \mathcal{T}} \|\mathbf{C}_{ab}\|_F \\ &\leq \max_{a \in \mathcal{T}} \sum_b \sum_c \|A_{ac}\|_F \|B_{cb}\|_F \\ &\leq \left\{ \max_{a \in \mathcal{T}} \sum_c \|A_{ac}\|_F \right\} \left\{ \max_{c \in \mathcal{T}} \sum_b \|B_{cb}\|_F \right\} \\ &= \|\mathcal{C}(A)\|_\infty \|\mathcal{C}(B)\|_\infty. \end{aligned}$$

□

Lemma 15.

$$\|\mathcal{C}(AB)\|_\infty \leq \|\mathcal{C}(A)\|_\infty \|\mathcal{C}(B)^T\|_\infty. \quad (41)$$

Proof. For a fixed a and b ,

$$\begin{aligned} \mathcal{C}(AB)_{ab} &= \left\| \sum_c A_{ac} B_{cb} \right\|_F \\ &\leq \sum_c \|A_{ac}\|_F \|B_{cb}\|_F \\ &\leq \max_c \|A_{ac}\|_F \sum_c \|B_{cb}\|_F. \end{aligned}$$

Maximizing over a and b gives the result. □

D Additional Information About Functional Brain Networks

Table 3 contains list of the names of the brain regions. The number before each region is used to index the node in the connectivity models. Figures 9, 10 and 11 contain adjacency matrices for the estimated graph structures.

Table 3: Names of the brain regions. L means that the brain region is located at the left hemisphere; R means right hemisphere.

1	Precentral_L	49	Fusiform_L
2	Precentral_R	50	Fusiform_R
3	Frontal_Sup_L	51	Postcentral_L
4	Frontal_Sup_R	52	Postcentral_R
5	Frontal_Sup_Orb_L	53	Parietal_Sup_L
6	Frontal_Sup_Orb_R	54	Parietal_Sup_R
7	Frontal_Mid_L	55	Parietal_Inf_L
8	Frontal_Mid_R	56	Parietal_Inf_R
9	Frontal_Mid_Orb_L	57	SupraMarginal_L
10	Frontal_Mid_Orb_R	58	SupraMarginal_R
11	Frontal_Inf_Oper_L	59	Angular_L
12	Frontal_Inf_Oper_R	60	Angular_R
13	Frontal_Inf_Tri_L	61	Precuneus_L
14	Frontal_Inf_Tri_R	62	Precuneus_R
15	Frontal_Inf_Orb_L	63	Paracentral_Lobule_L
16	Frontal_Inf_Orb_R	64	Paracentral_Lobule_R
17	Rolandic_Oper_L	65	Caudate_L
18	Rolandic_Oper_R	66	Caudate_R
19	Supp_Motor_Area_L	67	Putamen_L
20	Supp_Motor_Area_R	68	Putamen_R
21	Frontal_Sup_Medial_L	69	Thalamus_L
22	Frontal_Sup_Medial_R	70	Thalamus_R
23	Frontal_Med_Orb_L	71	Temporal_Sup_L
24	Frontal_Med_Orb_R	72	Temporal_Sup_R
25	Rectus_L	73	Temporal_Pole_Sup_L
26	Rectus_R	74	Temporal_Pole_Sup_R
27	Insula_L	75	Temporal_Mid_L
28	Insula_R	76	Temporal_Mid_R
29	Cingulum_Ant_L	77	Temporal_Pole_Mid_L
30	Cingulum_Ant_R	78	Temporal_Pole_Mid_R
31	Cingulum_Mid_L	79	Temporal_Inf_L
32	Cingulum_Mid_R	80	Temporal_Inf_R
33	Hippocampus_L	81	Cerebellum_Crus1_L
34	Hippocampus_R	82	Cerebellum_Crus1_R
35	ParaHippocampal_L	83	Cerebellum_Crus2_L
36	ParaHippocampal_R	84	Cerebellum_Crus2_R
37	Calcarine_L	85	Cerebellum_4_5_L
38	Calcarine_R	86	Cerebellum_4_5_R
39	Cuneus_L	87	Cerebellum_6_L
40	Cuneus_R	88	Cerebellum_6_R
41	Lingual_L	89	Cerebellum_7b_L
42	Lingual_R	90	Cerebellum_7b_R
43	Occipital_Sup_L	91	Cerebellum_8_L
44	Occipital_Sup_R	92	Cerebellum_8_R
45	Occipital_Mid_L	93	Cerebellum_9_L
46	Occipital_Mid_R	94	Cerebellum_9_R
47	Occipital_Inf_L	95	Vermis_4_5
48	Occipital_Inf_R		

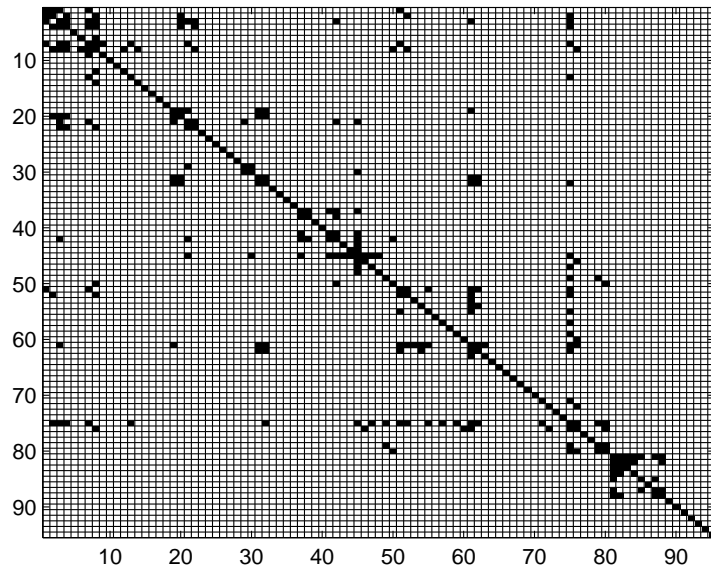


Figure 9: Adjacency matrix for the brain connectivity network: healthy subjects

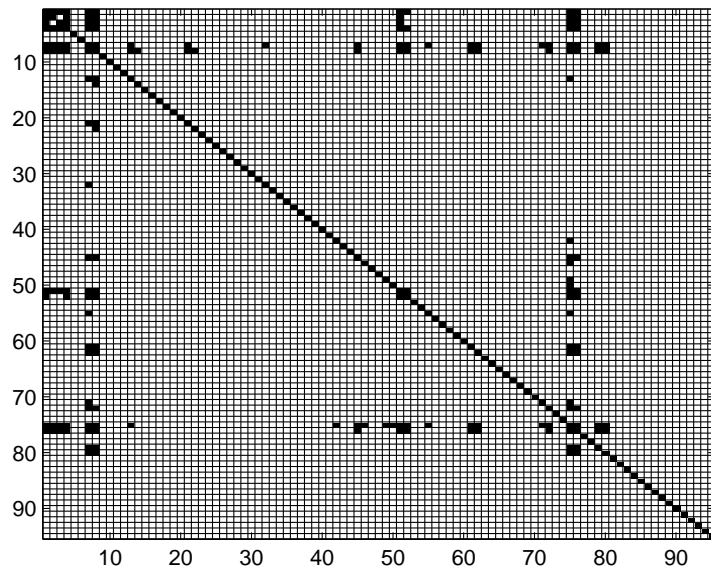


Figure 10: Adjacency matrix for the brain connectivity network: Mild Cognitive Impairment

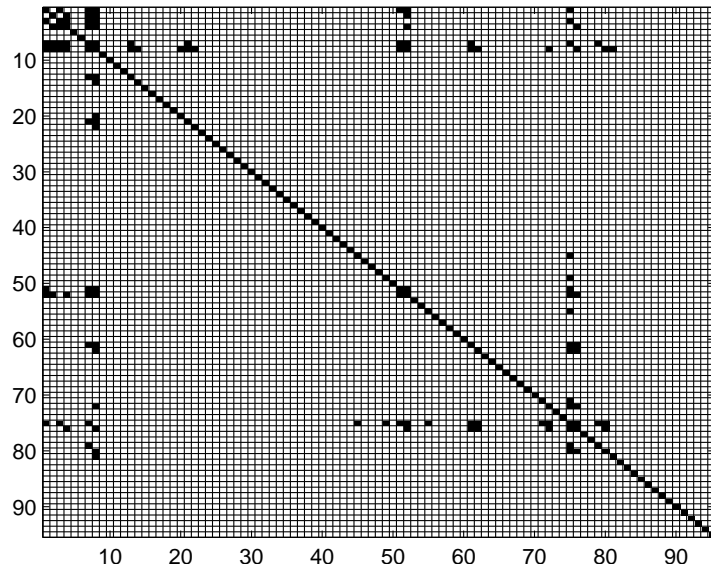


Figure 11: Adjacency matrix for the brain connectivity network: Alzheimer's & Dementia